

2017-01-01

Test Methods For The Fracture And Fatigue Crack Growth Behavior Of Hot Mix Asphalts

Eduardo Garcia

University of Texas at El Paso, egarcia14@gmail.com

Follow this and additional works at: https://digitalcommons.utep.edu/open_etd



Part of the [Engineering Mechanics Commons](#), and the [Mechanical Engineering Commons](#)

Recommended Citation

Garcia, Eduardo, "Test Methods For The Fracture And Fatigue Crack Growth Behavior Of Hot Mix Asphalts" (2017). *Open Access Theses & Dissertations*. 455.

https://digitalcommons.utep.edu/open_etd/455

This is brought to you for free and open access by DigitalCommons@UTEP. It has been accepted for inclusion in Open Access Theses & Dissertations by an authorized administrator of DigitalCommons@UTEP. For more information, please contact lweber@utep.edu.

TEST METHODS FOR THE FRACTURE AND
FATIGUE CRACK GROWTH BEHAVIOR OF HOT MIX ASPHALTS

EDUARDO GARCIA

Master's Program in Mechanical Engineering

APPROVED:

Calvin M. Stewart, Ph.D., Chair

Jack Chessa, Ph.D.

Soheil Nazarian, Ph.D.

Charles Ambler, Ph.D.
Dean of the Graduate School

Copyright ©

by

Eduardo Garcia

2017

Dedicado a mi familia

Mi madre, mi padre y mi hermana

Todo su esfuerzo, enseñanzas, y apoyo me han convertido en lo que soy

TEST METHOD FOR THE FRACTURE AND
FATIGUE CRACK GROWTH BEHAVIOR OF HOT MIX ASPHALTS

by

EDUARDO GARCIA, BSME

THESIS

Presented to the Faculty of the Graduate School of

The University of Texas at El Paso

in Partial Fulfillment

of the Requirements

for the Degree of

MASTER OF SCIENCE

Department of Mechanical Engineering

THE UNIVERSITY OF TEXAS AT EL PASO

August 2017

Acknowledgements

I would like to express my gratitude and respect to my advisor Dr. Calvin M. Stewart for his extensive guidance, leadership, and knowledge during my graduate years. He has taught me invaluable skills and has been truly rewarding working with such an advisor. I want to extend my gratitude to the Mechanical Engineering Department for providing me with the research opportunity and experience. I would like to express my appreciation to Dr. Jack Chessa and Dr. Soheil Nazarian for serving as my committee members and for their valuable feedback.

I would like to thank my college colleagues for their help and knowledge: Shafin Haque, Christopher Ramirez, William Chinedu, Victor Garcia, Alejandra Escajeda, Mauricio Valenzuela, Carlos Garcia, Ricardo Garcia, Alejandra Castellanos, Sergio Cordova, and Jesus Reyes. Thank you to all my friends that were with me throughout this journey, you have made it possible as well: Emilio Tarango, Jonathan Adame, Oscar Moreno, Carlos Ruiz, Ignacio Delgado, Eduardo Simental, John Paul Barreda, Jorge de la Rosa, and Fernando Trueba.

I warmly thank you Adriana Valdez, for your support and encouragement every single day love.

Por ultimo, quiero agradecer a mi familia, especialmente a mi madre quien ha hecho todo esto posible, siempre recordare tu apoyo.

Abstract

The service life and mechanical properties of bituminous mixtures are greatly affected by distress problems such as fracture, thermal cracking, and fatigue cracking of the asphalt layers. The fracture and fatigue crack growth (FCG) behavior of bituminous mixtures are difficult to quantify due to material-, test-, and equipment-related uncertainties. The goal of this study is to introduce a systematic fracture and fatigue crack growth testing approach for hot mix asphalts (HMAs). The objective is to experimentally evaluate the fracture resistance and fracture toughness behavior of a dense-graded HMA material at different temperatures and varying thicknesses. The effect of thickness on the fracture tests is investigated to identify plane-stress or plane-strain conditions. The FCG behavior for a single stress ratio and frequency at 5, 25, and 40°C is also evaluated and investigated. The tensile and fracture properties are recorded using indirect tension tests (IDT) and disk-shaped compact tension (DCT) tests. Disk compact tension specimens exhibit more advantages in evaluating cracking resistance and fracture behavior. Fracture toughness tests and load-controlled fatigue tests according to ASTM standards are performed. Digital image correlation (DIC) is employed to measure the crack length, determine the stress intensity factor for crack opening, and observe the stress fields on the plastic zones of the crack. Using linear elastic fracture mechanics (LEFM) the Paris, Walker, and Forman law material constants are determined and modeled to the experimental data to predict the linear crack growth region.

Table of Contents

Acknowledgements.....	v
Abstract.....	vi
Table of Contents.....	vii
List of Tables	ix
List of Figures.....	x
Chapter 1: Introduction	1
Evaluation of Fracture and Thickness Effect in Asphalts	1
Evaluation of Fatigue Crack Growth in Asphalts.....	8
Scope of Study.....	11
Chapter 2: Experimental Methods	12
Material.....	12
Specimen Preparation	13
Mechanical Test Equipment	15
3D Surface Scanning	16
Digital Image Correlation	16
Chapter 3: Methodology	20
Indirect Tensile Test	20
Fracture Resistance Tests	21
Fracture Energy Test.....	21
Fracture Toughness Test.....	21
Fatigue Crack Growth Rate Tests.....	26
Chapter 4: Fracture Test Results At Different Thickness.....	28
ASTM Requirement.....	28
Fracture Toughness.....	28

Fracture Energy	32
Crack Path.....	35
3D Surface Scanning	36
Chapter 5: Fracture And Fatigue Crack Growth Results At Different Temperatures	39
Indirect Tensile Strength.....	39
Fracture Energy Results.....	40
Fracture Toughness.....	42
Fatigue Crack Growth.....	46
Crack Tip Observations	52
Evolution of Strain Fields.....	54
Chapter 6: Summary And Conclusions.....	57
Future Work.....	59
References	60
Vita.....	64

List of Tables

Table 1 – Gradation chart of Type-C mix.....	12
Table 2 – Material properties of dense-graded (Type C) mix	13
Table 3 – Pre-cracking parameters	25
Table 4 – Fatigue crack growth test parameters	27
Table 5 – Tensile and Fracture Properties of HMA Type-C	39
Table 6 – Indirect tensile strength properties.....	40
Table 7 – Fracture energy properties	42
Table 8 – Fracture toughness properties	44
Table 9– Fatigue crack growth test conditions	47
Table 10– Fatigue Crack Growth Results	50
Table 11 – Fracture Toughness of Dense-Graded HMA	30
Table 12 – Fracture Energy of Dense-Graded HMA.....	33

List of Figures

Figure 1 - Fracture in heterogeneous particulate composite.....	3
Figure 2 - Climate variability in southern regions depicting (a) high temperature low humidity and (b) low temperature and high humidity.	4
Figure 3 - Fracture toughness and fracture surface versus thickness in homogeneous linear-elastic materials.....	6
Figure 4 – Disk-shaped compact tension (DCT) (a) specimen and (b) dimensions	13
Figure 5 – Indirect tension (IDT) specimen a) specimen and b) dimensions	13
Figure 6 – Mechanical setup a) Instron 5969 Table-top and b) MTS 810 Universal Test System (UTM).....	15
Figure 7 - DIC specimen preparation.....	17
Figure 8 – DIC schematic	18
Figure 9 – Crack length measurement method along tortuous path	19
Figure 10 – Precracked specimen according to $0.1B$ requirements.....	23
Figure 11 – Types of Force-Displacement Records [5].....	25
Figure 12 - Schematic sigmoidal behavior of fatigue crack growth versus ΔK	26
Figure 13 - IDT (a) strength-displacement curves and (b) strength with COV	40
Figure 14 - Fracture energy (a) load-CMOD curves and (b) strength with COV.....	42
Figure 15 - Fracture toughness (a) load-CMOD curves and (b) strength with COV	45
Figure 16 - Fracture toughness behavior at different temperatures.	45
Figure 17 - Early failure at the loading grips for the 40 °C fatigue crack growth tests.	47
Figure 18 – Fatigue crack length versus cycles at each temperature.....	48
Figure 19 - Fatigue crack growth rate versus stress intensity range at (a) 5 and (b) 25 °C	49
Figure 20 – Vertical strain E_{yy} at crack tip at maximum load during fracture toughness tests at 5, 25, and 40 °C.....	52
Figure 21 – Vertical strain evolution E_{yy} at different fatigue life percent N_f in specimen at 5 and 25 °C respectively.	54
Figure 22 – Load-displacement curves of fracture toughness tests at thicknesses from (a) 25 to (d) 75 mm respectively.....	31
Figure 23 – Peak load versus critical crack length	31
Figure 24 – Fracture toughness versus thickness: (a) magnitude and (b) coefficient of variation.....	32
Figure 25 – Load-CMOD curves of fracture energy tests at thicknesses from (a) 25 to (d) 75 mm respectively	34
Figure 26 – Fracture energy versus thickness: (a) magnitude and (b) coefficient of variation	34
Figure 27 – Crack Path observed in K_c specimen	35
Figure 28 – Crack Path observed in G_f specimen.....	36
Figure 29 – 3D Fracture Surface at specimen thicknesses from 25 to 75 mm	38

Chapter 1: Introduction

Asphalt pavements are subjected to cyclic traffic loads during their service life. The repeated load in addition to climate changes induces fatigue cracking on the surface layers of these materials. Several forms of distress problems in asphalt pavements include fracture, thermal cracking, reflective cracking of the asphalt layer, and most importantly fatigue cracking [1-4].

Evaluation of Fracture and Thickness Effect in Asphalts

As the thickness of a geometry changes, the material property transition from plane stress to mixed mode to plane strain during fracture resistance tests. Plane stress and plane strain conditions differ in the way that plane stress absorbs more energy than plane strain during cracking making the fracture properties and process significantly different [5]. During plane strain conditions failure energy remains constant and therefore becomes independent of specimen thickness. Disk compact tension geometry is standardized in ASTM E399 “Standard test method for plain-strain fracture toughness in Metallic materials” for metallic materials. Similarly, ASTM E1820 “Standard Test Method for Measurement of Fracture Toughness” stipulates width to thickness ratio (W/B) suitable for homogenous materials only. Fracture toughness K_{ic} within the tested width to thickness ratio (W/B) is not an intrinsic material property until plane strain is attained [6]. Despite these challenges, researchers still employ both ASTM E1820 and ASTM E399 as a valid standard for heterogeneous materials like hot mix asphalts (HMAs). Thus, reinforcing the difficulty in the repeatability of fracture resistant tests and determining the fracture energy G_f and fracture toughness K_{ic} as the true material property.

Hot mix asphalts (HMAs) consist on one of the highest strength alternatives for asphalt pavement surface layers composed mainly with a bitumen and an aggregate [7]. The aggregate (particulates) consist of crushed stone, sand, and mineral that are distributed with different sizes and spatial random distributions along the binder. The stone particles are brittle and act in an elastic-perfect plastic mechanical response [8]. The binder component exhibits viscoelastic response and thermoplastic behavior because of the interaction of constituents in the heterogeneous particulate composite. This viscoelastic behavior displays elastic response and high strength during fast loading conditions and low strength at slow loading conditions. Thermoplastic behavior is characterized as the low strength during high temperatures and high strength in low temperatures [7]. The fracture mechanisms of HMAs are like those observed in heterogeneous particulate composites where interfacial bond energy plays an important role in cracking phenomena. During cracking and permanent deformation, the stress, strain, and damage zones are localized around the aggregates. The primary crack exhibits cracking bridging ahead of the crack tip and a traction free crack behind the crack tip as depicted in Figure 1. At lower temperatures, the cracking tends to propagate through both the aggregates and binder whereas at high temperatures, the crack propagates around the aggregates increasing the potential of aggregate interlocking and bridging [9]. The particulate sizes influence in the repeatability of fracture and fatigue tests due to the randomness in distribution and difference in size that produces variation in mechanical response within the aggregate-binder interfaces. An understanding and measurement of the engineering properties of these asphalt mixtures consist of a broad scope of specifications for design and analysis [3].

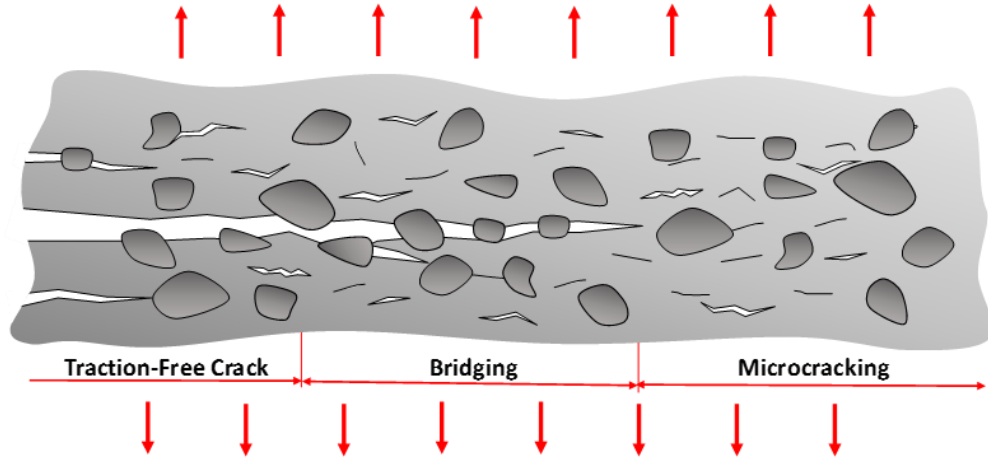


Figure 1 - Fracture in heterogeneous particulate composite.

The dominant fracture mechanism in HMAs is micro-crack nucleation and growth within the asphalt mixture at the binder-aggregate interfaces [10]. The size of the plastic zone ahead of the crack tip in these failures exceeds the plasticity limitation of linear-elastic fracture mechanics (LEFM) [11]; However, the use of LEFM is still a fitting method to evaluate the fracture toughness K_{ic} and fracture energy G_{ic} of bituminous mixtures considering the crack tip stress fields [12,13-18]. The fracture toughness, K_c is an intrinsic property of the material that is independent of specimen thickness under plane strain conditions called the plane-strain fracture toughness, K_{ic} . Plane strain can be identified when examining a fracture toughness versus thickness plot. There exists a critical thickness above which fracture toughness becomes constant and insensitivity to size. This condition is plane strain. When thickness is less than the critical value, the plane stress condition is observed. Under plane stress, the material absorbs more energy and microstructural defects play a dominant role in the fracture resistance leading to an inconsistent fracture toughness, K_c and coefficient of variation that changes with respect to thickness [5]. Plane stress should be avoided.

The elastic plastic fracture mechanics (EPFM) is another approach developed for fracture assessment where the crack fracture zone is larger due to temperature effects and critical energy rate J_{ic} and J integral are introduced [18]. In general, fracture energy, G_f is insensitive to thickness as the work of fracture (energy) is normalized by thickness; however, the coefficient of variation is not. Asphalt pavements are subject to an extensive range of temperatures. LEFM is not valid at elevated temperature where HMAs exhibit a visco-elastic-plastic behavior. An alternative indices for fracture resistance is required. In EPFM a large plastic zone at the crack tip can be encapsulated by the J -integral a contour integral of the local strain energy. Once a critical strain energy release rate is reached, J_{ic} , fracture occurs [18]. The heterogeneous microstructure of HMAs makes the calculation of the J -integral and subsequent measurement of J_{ic} challenging. Despite these requirements, indices to evaluate fracture toughness at high temperatures are scarce. Climate extremes can significantly impact the surface transportation infrastructure. In the southern plains region, extreme climate across the spectrum from subzero to triple digit temperature and high-low humidity are observed as shown in Figure 2.



Figure 2 - Climate variability in southern regions depicting (a) high temperature low humidity and (b) low temperature and high humidity.

Several researchers have investigated the fracture resistance of asphalt mixtures [1, 9, 12, 11, 13, 6, 5, 18, 19- 23, 24]. The semi-circular bending (SCB) test is a common fracture test for

HMAAs due to the simplicity of specimen preparation and testing [21]. Saha and Biligiri conducted a review of the state-of-the-art concerning SCB testing of asphalt mixtures [6]. Current standards recommend a specimen thickness of 50 mm [24, 23]. Both the fracture toughness, K_c and fracture energy, G_f parameters were evaluated. Fracture toughness, K_c was found to be independent of thickness between 25 to 75 mm at temperatures below 15°C; however, as temperature increases the magnitude of K_c decreases and the COV increases. Fracture energy, G_f was determined to be dependent on asphalt grade and temperature; however, the effect of thickness was not discussed. In theory, G_f of homogenous linear-elastic materials is insensitive to size; however, HMAAs are heterogeneous viscoelastic-plastic materials. In a follow-on study, Saha and Biligiri [5] evaluated the homothetic fracture resistance behavior of dense grade HMA materials (i.e. the dependence on asphalt content, air voids, temperature, and thickness) using the SCB test. Tests were performed at temperatures of 5 to 25°C with thicknesses from 30 to 50 mm. Increasing the thickness from 30 to 40 mm increased the K_c ; however, thicknesses from 40 to 50 mm exhibited little to no change in K_c . Arabani and Ferdowsi, examined the feasibility of SCB and IDT tests on asphalt materials of different grades, thicknesses and binder contents. Tests were performed on thicknesses ranging from 25 mm to 75 mm and diameter of 100 mm and 200 mm. Comparing variation of fracture toughness and tensile strength, results from the employed tests revealed that fracture toughness is more dependent of gradation than binder content but independent on thickness [25]. Several researchers, have also measured the mixed-mode fracture resistance of HMAAs in the SCB configuration [1, 13].

Specimen geometry plays a key role K_c . Stewart et al. [11] in performed a comparative analysis of the SCB and disk-shaped compact tension (DCT) fracture energy test standards on a

dense-graded Superpave HMA. The SCB and DCT tests were conducted according to AASHTO TP105-13 and ASTM D7313-13 at the recommended thickness of 50 mm and a temperature of 27°C [24, 23]. The SCB tests produced a low fracture energy with a high COV when compared to DCT. They determined that the DCT geometry offered more fracture area for cracking propagation making it a more repeatable test.

Wagoner et al. [9] performed DCT fracture energy tests on four asphalt mixtures ranging from typical Illinois to polymer-modified interlayer mixtures. For a single mixture at -10°C, the thickness was profiled from 25 to 75 mm. Fracture energy, G_f was found to increase with thickness while the COV also increased from 13 to 19%. Kim et al. [12] found that increasing the diameter of a specimen from 100 to 450 mm led to an increase in G_f while the COV remained relatively constant near 15%.

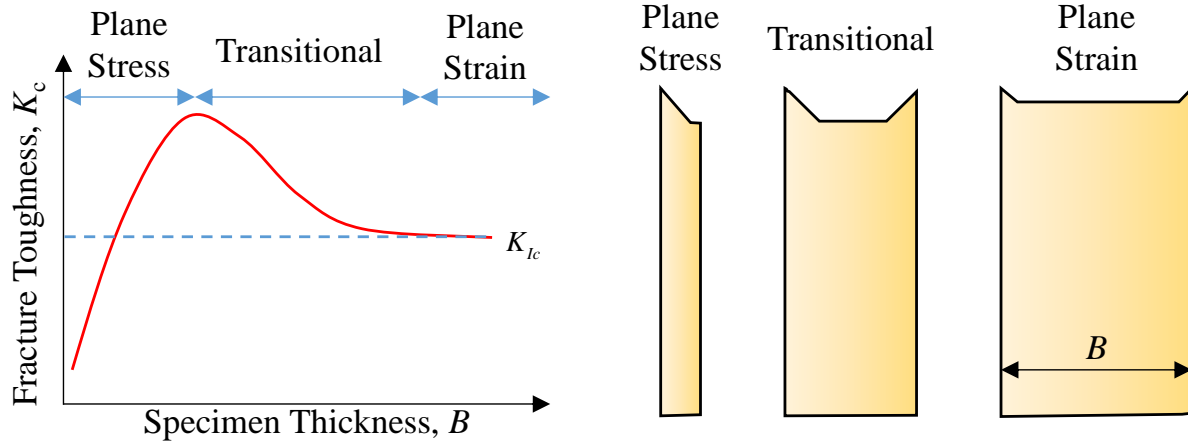


Figure 3 - Fracture toughness and fracture surface versus thickness in homogeneous linear-elastic materials

According to linear-elastic fracture mechanics (LEFM) theory, fracture toughness of a homogeneous material is thickness dependent up to the plane-strain condition where the value becomes a constant material property [22]. The size or thickness dependence is associated with the transition from plane-stress to plane strain as illustrated in Figure 3. The fracture toughness, K_c is

called the “apparent” fracture toughness when it is thickness-dependent and is called the “plane-strain” fracture toughness, K_{ic} when it becomes an intrinsic material property that is not thickness-dependent. In plane-stress, the direction of maximum shear stress is in the anti-plane direction ($\pm 45^\circ$) leading to the formation of a slant crack or shear lips. Microstructural defects play a significant role in fracture toughness resulting in a high COV. As thickness increases, the specimen transitions from plane-stress to a plane-strain condition. In plane-strain, the direction of the maximum shear stress is in-plane leading to a flat fracture surface. The field of defects in the material homogenize such that the fracture toughness resolves to a horizontal asymptote with a low COV. By reviewing LEFM theory, it can be concluded that

- the plane-strain fracture toughness, K_{ic} is a conservative measure of fracture resistance.
- for design it would be advantageous to determine the thickness where the apparent fracture toughness, K_c is maximized and the COV is reasonable.

Since HMAs are heterogeneous composites, and the theory described above may not hold true, there is a need to investigate the apparent fracture toughness to the actual plane-strain fracture toughness relationship for HMAs.

It is important to check the ASTM requirements for the plane-strain condition. ASTM developed two standards to support the measurement of the K_{ic} in metallic and homogenous materials: ASTM E399-12e3 [26] and ASTM E1820-16 [27], respectively. A key requirement of these two standards is that the width-to-thickness ratio, W/B , shall remain between 2 and 4. The standard ratio is $W/B = 2$. Another requirement is that the following inequality be enforced

$$a, B \geq 2.5 \left(\frac{K_{ic}}{\sigma_{YS}} \right)^2 \quad (1)$$

where K_{ic} is the approximate plane-strain fracture toughness, σ_{ys} is the yield strength, a is the crack length, and B is the thickness. The fracture toughness cannot be considered plane-strain, K_{ic} , when this condition is violated, and it must be defined as the apparent fracture toughness, K_c , reported everywhere with respect to thickness [6].

Evaluation of Fatigue Crack Growth in Asphalts

The primary form of failure in asphalt concrete pavements is the fatigue cracking and it is often difficult to predict due to the poor repeatability of fracture and fatigue tests driven by (a) the poor quality of existing test standard and (b) the heterogeneous nature of the material with randomly distributed particles in a bituminous mixture [28]. Fatigue damage at the particle-binder interface occurs at relative low alternating stress magnitudes eventually leading to the service failure or breakage of asphalt mixtures. The fracture resistance, fatigue life, and fatigue crack growth behavior can greatly affect the durability and service life of pavements. There have been many studies conducted on the development of new materials and fatigue and fracture tests to assess and better understand the complex fatigue phenomenon and cracking mechanisms in bituminous mixtures [9,12,29-32].

The indirect tensile tests (IDT), flexural beam and bending tests, and semicircular bending tests (SCB) have been widely used to determine the fatigue crack growth and fatigue behavior of asphalt mixtures [4, 2, 33, 34].

Saha and Biligri investigated the homothetic behavior of asphalt mixes with respect to fracture toughness, K_c , using SCB tests of six dense graded asphalt mixes at 5, 15, and 25 °C with sample thicknesses of 30, 40, and 50 mm [5]. Fracture toughness was profiled with respect to temperature, asphalt content, air void percentage, and thickness. The plane strain condition was observed at thickness greater than 40mm. Asphalt content, air voids, and temperature were observed to have

little impact on the plane strain condition at thickness between 40 and 50 mm. Kim and colleagues developed a discrete element method (DEM) based numerical model to simulate crack initiation and propagation in asphalt mixtures [12]. To calibrate the model, DCT tests were performed on a superpave NMAAS mixture following ASTM E399 with a fixed specimen thickness of 50mm and diameter varying from 100 to 450 mm at -10 °C with different crack mouth opening displacements (CMOD) depending on size. The average fracture energy, G_f recorded during the experiments was observed to increase with diameter while the coefficient of variation remained high (>15%) and insensitive to diameter. By replicating the heterogeneous microstructure of the material, the numerical model was able to match the experimental force vs CMOD curves [12]. Stewart and colleagues performed a comparative analysis of the SCB and DCT fracture resistance test standards on a superpave Type-D mixture using 3D-DIC strain fields and a 3D surface scanner. The SCB and DCT tests were done according to AASHTO TP105-13 and ASTM D7313-13 respectively at room temperature. The SCB tests produced a low average fracture energy with a high coefficient of variation (COV) when compared to DCT. The DCT geometry offers more fracture area for cracking propagation making it a more repeatable and reliable test [11].

Nejad and colleagues investigated the elastic modulus and fatigue lives in terms of aggregate sizes, coarseness, temperature, and asphalt content in HMA and stone matrix asphalt (SMA) mixtures using fatigue prediction equations [4]. Both IDT elastic modulus and fatigue tests were carried out under load-control at stress amplitudes, σ_a from 30 to 1000 kPa at 5, 25, and 40 °C respectively. It was concluded that increasing the temperature will decrease the elastic modulus and fatigue life of asphalt mixture independently from gradation type, asphalt content, and other factors. Mixtures with fine gradation exhibit superior fatigue performance to those with coarse gradation. Khiavi and Ameri researched the fatigue endurance limit at low strain levels using the

ratio of dissipated energy change (RDEC) approach and the plateau value at 50% stiffness reduction ($PV-N_{f50}$) relationship [33]. Four-point beam fatigue test were conducted following AASTHO T321 using semi-sinusoidal loading at 10 Hz for 7 strain levels. This study concluded that there exists a transition point in the log strain- N_{f50} curve and that the cycles corresponding to the transition strains are different than the cycles corresponding to the plateau value endurance limit, PV_L .

Tschegg and colleagues studied the fatigue crack growth performance on solid asphalt and asphalt-asphalt interfaces using wedge splitting test [2]. Tests under load-control with a sinusoidal waveform at a frequency of 2 Hz were performed at -10, 0, and +10 °C respectively with an initial load amplitude equal to 70% of notch tensile strength. The crack growth rates (measured using optical methods) were observed to be 10 times faster at +10 °C when compared to 0 °C and 100 times faster at +10 °C when compared to -10 °C. While the semicircular bending test (SCB) has been widely used to determine the fracture mechanisms of HMAs, the disk compact tension test (DCT) exhibits more advantages in evaluating the fracture toughness and energy, fatigue-life, and fatigue crack growth of asphalt mixtures [9, 11, 16]. DCT is recommended as reported by the Investigation of Low Temperature Cracking in Asphalt Pavements National Pooled Fund Study to be the test method to calculate fracture testing due to more consistent and accurate results, large ligament area for cracking propagation, and existence of ASTM standards in that configuration [17].

As described above, a large variety of specimen geometry, test standards, and analyze approaches have been performed to assess the fracture, fatigue, and fatigue crack growth behavior of HMAs. Disagreement at state-, country-, and international-level organizations makes the development of a standard protocol for these phenomena challenging. There is a constant research

to develop testing methods to improve repeatable and reproducible test standards that identify and mitigate the material-, test-, and equipment-related uncertainties. In this study, a new fatigue crack growth procedure for HMAs is introduced by adopting the rules and restrictions found in FCG testing standards for metallic materials. Most standards and fracture calculations of asphalt mixtures are derived from metallic materials. Fatigue cracking is an important form of distress in these materials and the repeatability of results to improve the COV to better quantify this phenomena is a common research topic in the asphalt mixtures field.

Scope of Study

The main goal of this thesis study is to propose a testing methodology to characterize and evaluate the fatigue crack behavior and observe the effect of thickness in fracture tests in HMAs. Develop a testing method using the disk compact tension (DCT) specimen geometry to characterize fracture toughness and fatigue crack growth data based on LEFM assumptions with consistent COV values and repeatable results, reliable approach, and applicable to hot mix asphalts.

A systematic and rigorous methodology was conducted to achieve the following objectives:

- Experimentally evaluate and determine the fracture and fatigue parameters following ASTM standards applied to metallic materials but modified for asphalt mixtures.
- Examine the homothetic behavior by varying the thickness to determine the fracture properties.
- Examine the thermoplastic behavior using fracture and fatigue tests with respect to fracture toughness K_{ic} at varying temperatures based on LEFM assumptions.

Chapter 2: Experimental Methods

Material

The subject material of this study is a dense-graded hot mix asphalt (designated as Type-C by Texas Department of Transportation) used in West Texas. The aggregates and asphalt were tested in accordance with ASTM, AASHTO, and Texas Department of Transportation (TxDOT). The asphalt was delivered to the Center for Transportation Infrastructure Systems at the University of Texas at El Paso (UTEP) for specimen preparation, testing, and analysis. The gradation of the mix is shown in Table 1. The asphalt performance grade, binder substitution, asphalt content, and other material properties are shown in Table 2. A general distribution of mineral aggregate, asphalt binder, and air voids can be observed in a sample specimen in Figure 4a. According to the binder substitute, this material is often employed in 55 mph highways. This binder meets high temperature physical properties up to 64 °C and meets low temperature physical properties down to -22 °C.

Table 1 – Gradation chart of Type-C mix

Sieve Size	Type-C (Percentage)
1''	100.0
3/4''	99.3
3/8''	82.4
No.4	52.7
No. 8	36.9
No. 30	18.6
No. 50	14.0
No. 200	5.6

Table 2 – Material properties of dense-graded (Type C) mix

Properties	Type-C
Asphalt Performance Grade	PG 70-22
Binder Substitution	PG 64-22
Optimal Asphalt Content (%)	4.7
Specific Gravity	1.001
Binder Percent (%)	4.6
VMA (%) at optimum AC	15.2

Specimen Preparation

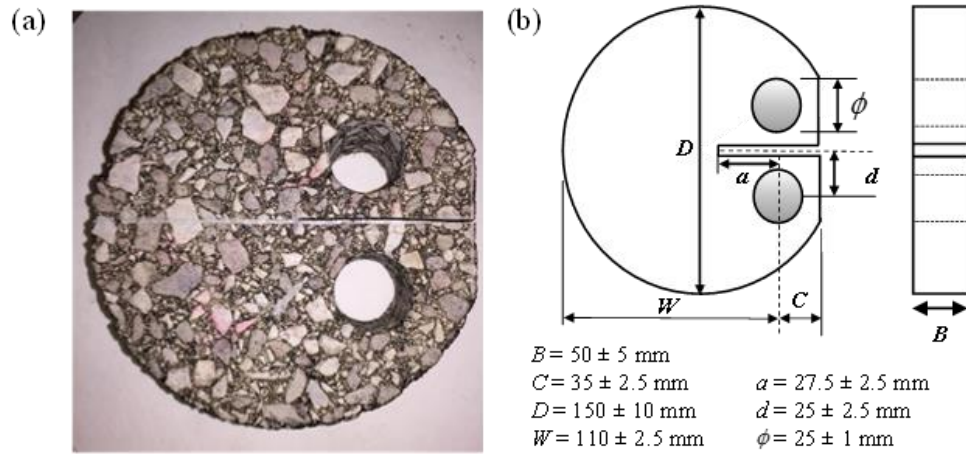


Figure 4 – Disk-shaped compact tension (DCT) (a) specimen and (b) dimensions

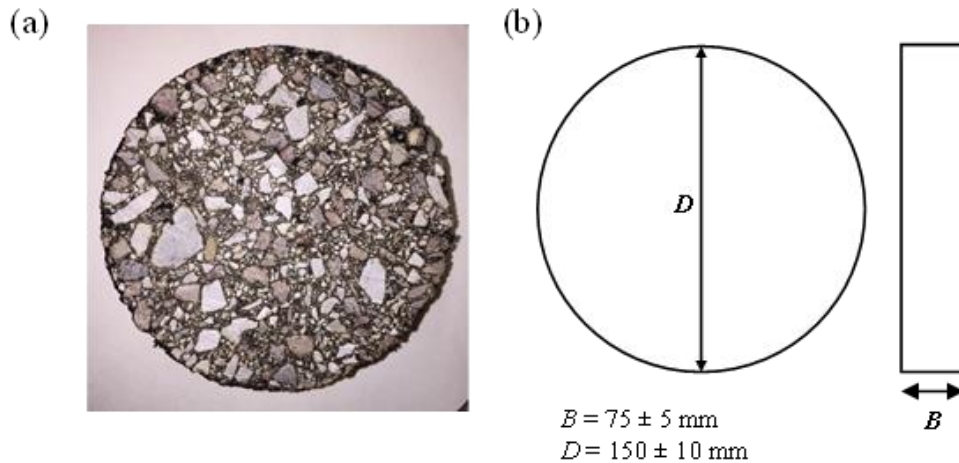


Figure 5 – Indirect tension (IDT) specimen a) specimen and b) dimensions

Two types of specimen were prepared for this study: disk-shaped compact tension (DCT) and indirect tension (IDT) as depicted in Figure 4 and Figure 5 respectively. The dimensions of these specimens are illustrated in Figure 4b and Figure 5b respectively. The specimens were manufactured according to AASHTO T312-15 and ASTM D6928-15 [35, 36]. The mixture was heated to 121.1 °C (250 F) and held at a constant temperature for 3 hours after which the material was compacted with a superpave gyratory compactor at a height of 115 ± 10 mm creating a HMA core. The mixture is then conditioned to room temperature before preparation.

At this point, either an IDT or DCT specimen can be prepared. For IDT, a cylindrical disk is excised from the middle of the HMA core at a thickness of 75 ± 5 mm. This is the last step for IDT. For DCT, the disk is excised at a thickness of 50 ± 5 mm. Specimen were prepared with thicknesses of 25, 40, 50, and 75 mm. The width-to-thickness range is $1.46 \leq W/B \leq 4.4$. The crack mouth, loading holes, and notch are fabricated using a water-cooled saw to avoid damaging the specimens in accordance to ASTM 7313-13 [24]. After this procedure, the machined notched is sharpened using a razor blade. This is done to prevent crack bifurcation during pre-cracking.

Mechanical Test Equipment

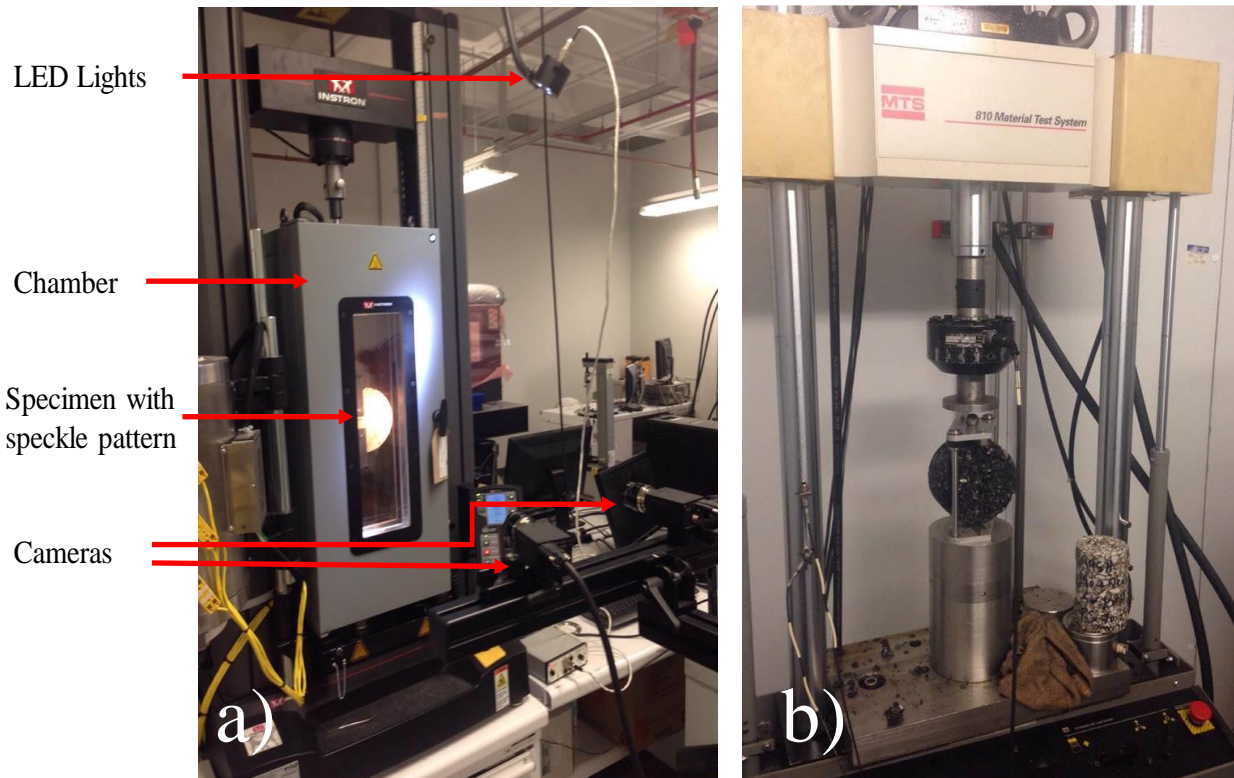


Figure 6 – Mechanical setup a) Instron 5969 Table-top and b) MTS 810 Universal Test System (UTM)

The IDT tests were conducted on a MTS 810 Universal Test System (UTM) while the DCT specimens were conducted on a Instron 5969 Table-top UTM. The Instron is configured with a 3119-609 environmental chamber enabling temperature control from -100 to +350 °C as seen in Figure 6a. The electro-mechanical Instron 5969 test frame is capable of 0.001 to 600 mm/min displacement rates, and is equipped with a 50 kN load cell. The servo-hydraulic MTS 810 is equipped with an 11-kip load cell and is inside an environmental room chamber as shown in Figure 6b. Load and displacement limits were set for the load cell, crosshead displacement, and extensometers to avoid equipment damage. The specimen are heated/cooled to an isothermal set temperature for the duration of each test. Time, load, load-line displacement, and high-resolution digital images are acquired from both test frames.

3D Surface Scanning

The fractured specimens are 3D scanned to produce a 3D CAD replication of the fracture surface using a MakerBot Digitizer 3D Scanner. The scanner has a nominal dimensional accuracy of ± 2 mm and detail resolution of 0.5 mm. The device uses two lasers and a rotating platform to generate a 3D dimensional replication of the surface of 3D objects. The Makerware software, exports a stereo lithography format file (.STL). The Autodesk MeshMixer software is employed to analyze the physical features of the 3-D .STL files.

Digital Image Correlation

Three-dimensional digital image correlation (3D DIC) is performed using DIC software VIC-3D and VIC-Gauge developed by Correlated Solution, Inc. The evolution of the strain fields on the surface of FCG specimen during tests was calculated using the VIC-3D software. Specimens were prepared with a random speckle pattern by the spray-paint method. These speckles create subsets that the software tracks. The software calculates the displacements (u , v , and w) and subsequently the strain vector and principal strains on the surface of the specimen. Calibration is performed prior to each test where a reference photo is taken of a calibration square (placed just in front of the specimen) to provide a physical reference of the distance and dimensions.

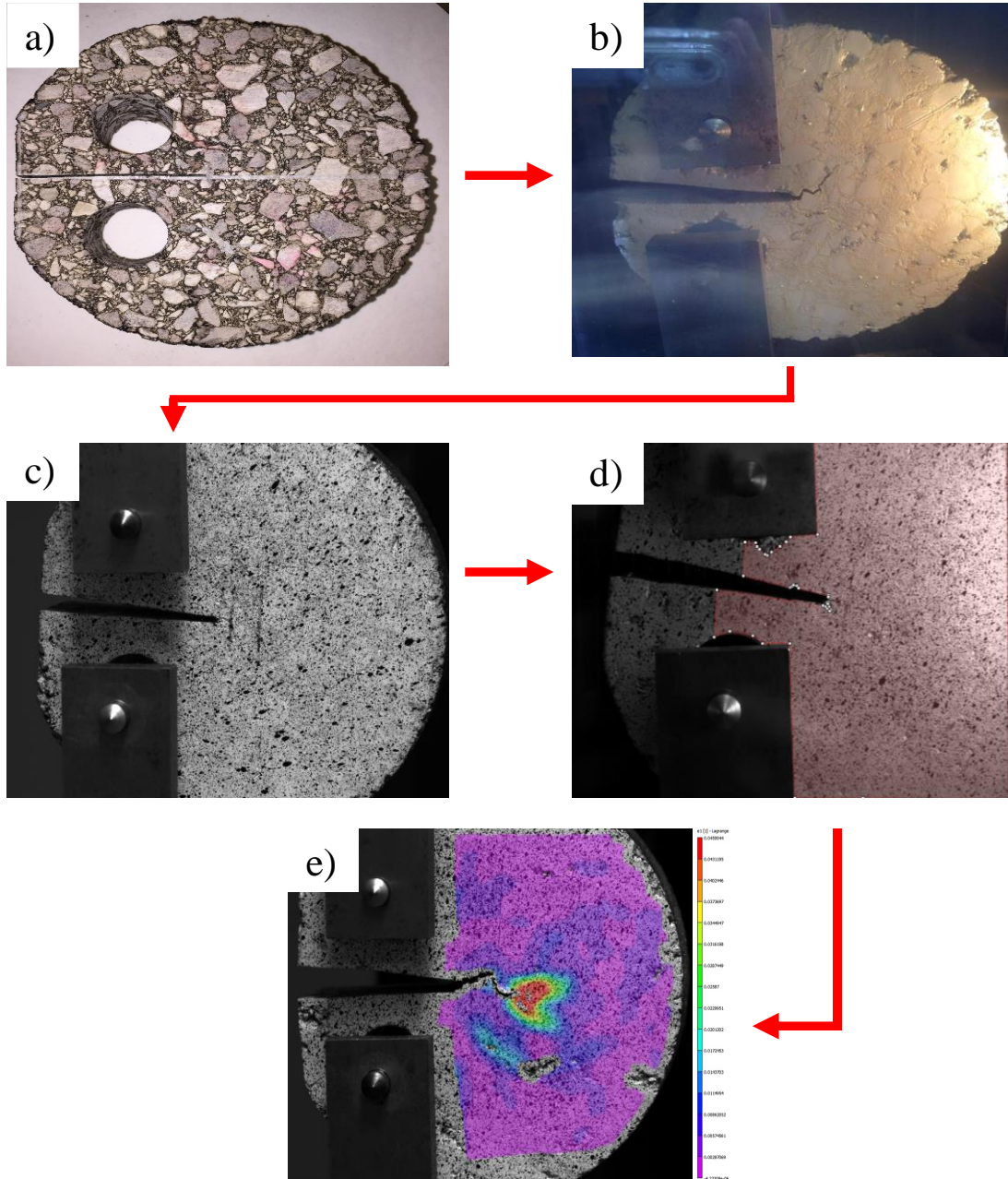


Figure 7 - DIC specimen preparation.

The specimen procedure for DIC is shown in Figure 7. Specimens were prepared with a white background for pre-cracking procedure and easier appreciation of the crack. Then a random speckle pattern was used by spray method which acts as the reference points. This procedure is crucial aspect for DIC. The pattern must be random and sized accordingly to the size of the specimen that is being tested. These points create subsets that the software tracks to process the

image correlation. A pre-calibration is then performed with several pictures and calibration card. The size of the calibration card must be appropriate for the size of the surface of the speckled pattern and covering as much of the object being tested. These pictures are then processed in the Vic-3D software so displacements and distances are measured. Light is another important factor for the calibration process since too much or too little light can affect a satisfactory calibration. Calibration images at room temperature were done using the laboratory light and high/low temperature calibration images were done aided by the light within the environmental chamber.

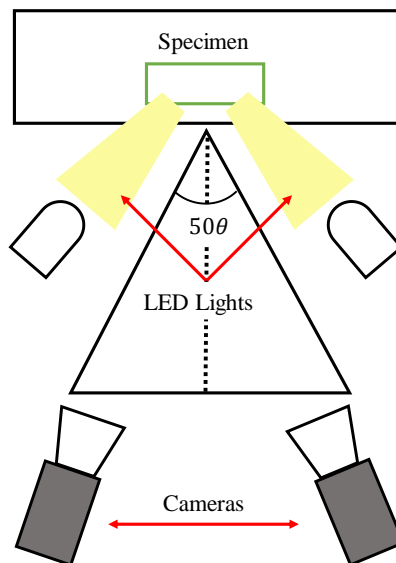


Figure 8 – DIC schematic

Digital image correlation setup consists of two 17-mm lens cameras and two tunable LED lights focused on the specimen to create contrast and accurately process the correlation. These cameras are precisely leveled and inclined at an angle of 25° or greater. During setup, light should be positioned in a way it does not shine directly onto the specimen. Once cameras are leveled, focused, and light is set, the setup cannot be changed nor modify during the series of test within that calibration process. Series of tests are performed with successful calibration set up every time. The equipment setup and schematic are shown in Figure 8.

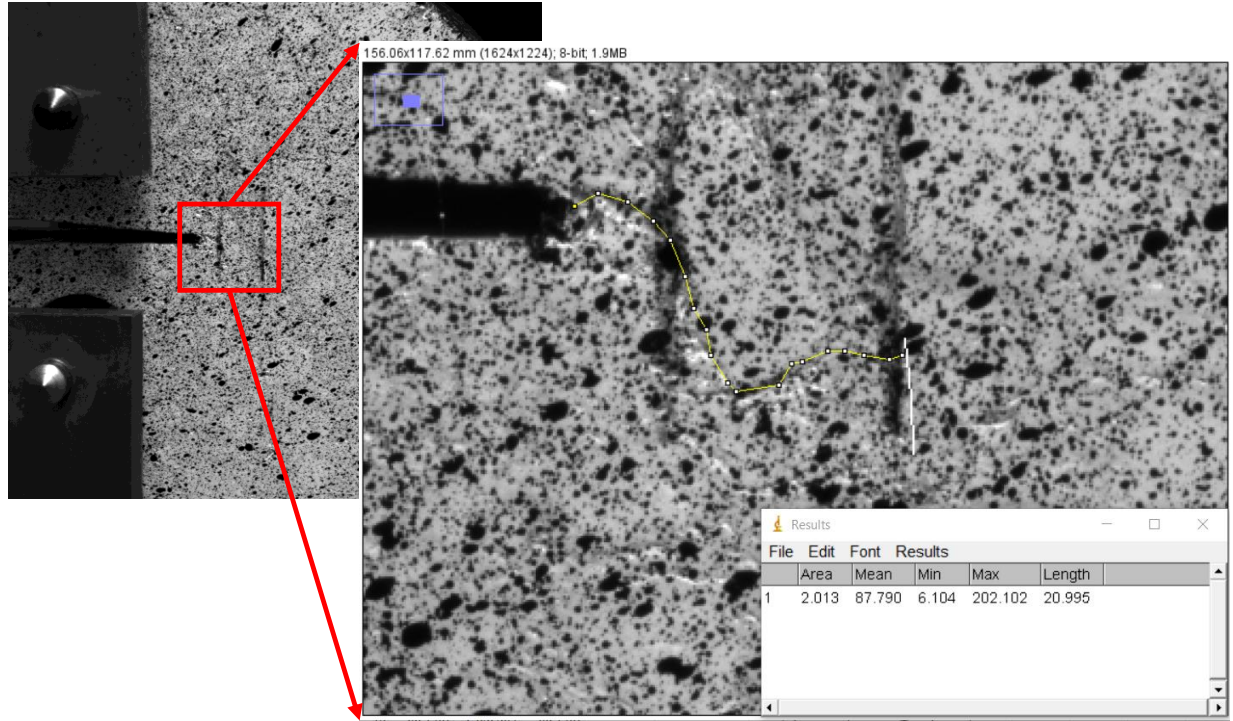


Figure 9 – Crack length measurement method along tortuous path

In this study, the crack length is measured continuously during the FCG tests. The photos collected using VIC-Snap at a frequency of 0.1 Hz and analyzed using Image J [37]. Photo capture was performed every 10-sec meaning there was one picture every cycle during the pre-cracking and FCG testing. The interval of data points captured by the Instron machine was every second. Measurement of the crack length was done every $\sim 50 \pm 5$ cycles where the load was at the peak of the cycle to ensure the largest crack measurement at the time. The crack was then traced in each image following the tortuous path to better approximate the true crack length as shown in Figure 9. Calibration of the scale was applied utilizing a known measure within the image (pre-cracking limit lines on the specimen equal to 5 and 10 mm). Photos were taken at one face of the specimen due to the back side of the chamber being covered.

Chapter 3: Methodology

The characterization of hot mix asphalts is a difficult task in which current studies and new developed testing methods are still on going. Due to the heterogeneous material composed of particulates at separate random distributions with different sizes and materials it is often difficult to quantify and evaluate the fracture and fatigue for asphalt mixtures. There have been several studies regarding the testing and quantification for asphalt mixtures, however, many of them still lack a clear procedure and detailed description to improve repeatability of results. In this study, a new test method for fracture and fatigue crack growth is introduced. Regarding fracture, a new pre-cracking procedure is adopted while following the validation requirements of specific ASTM standards based on metallic materials. Regarding fatigue crack growth, the use of disk compact tension specimen is employed which demonstrates more reliable and repeatable results in comparison with other specimen geometries. ASTM standard validation requirements are also followed for these tests.

Indirect Tensile Test

The indirect tensile tests (IDT) were conducted to determine the tensile strength of the asphalt mixture according to the ASTM D6931-12 for the “... Indirect Tensile (IDT) Strength of Bituminous Mixtures” [43]. The tensile strength is needed to decide on the applicability and tests parameters of fracture toughness and fatigue crack growth tests. During IDT test, load is applied on the vertical diametral plane of the specimen at a constant displacement rate until rupture or load drop below 40 N. In this study, the IDT tests were run on the MTS 810 UTS at a displacement rate of 50 mm/min at three isothermal set temperatures; 40, 25, and 5 °C respectively. The IDT strength is calculated as follows

$$S_t = \frac{2P}{\pi BD} \quad (2)$$

where S_t is IDT strength, P is the maximum load, B is the specimen thickness before testing, and D is the specimen diameter.

Fracture Resistance Tests

Fracture resistance test were performed on DCT specimen to measure both the fracture energy and fracture toughness. For fracture energy, an established testing standard is followed. For fracture toughness, the standard for metallic materials is adopted.

Fracture Energy Test

The DCT specimens were subjected to fracture energy tests according to ASTM 7313-13 for asphalt-aggregates mixtures [24]. The DCT tests are started at a seating load of no more than 0.2 kN (45 lbf). These tests are performed at a constant crack mouth opening displacement (CMOD) of 0.017 mm/s at isothermal set temperatures of 40, 25, and 5°C respectively. Fracture energy tests are stopped when the post-peak load reaches less than 0.1 kN. The fracture energy, G_f is calculated as follows

$$G_f = \frac{W_f}{B \cdot (W - a)} \quad (3)$$

where W_f is work of fracture or area below DCT curve, B is the thickness of the specimen, and $(W - a)$ is the initial ligament length.

Fracture Toughness Test

To characterize the fracture toughness, the ASTM E399-12 standard for the “... Linear-Elastic Plane-Strain Fracture Toughness K_{Ic} of Metallic Materials” is adopted with some

modification [26]. The specimen dimensions were kept to ASTM 7313-13 since it is specific to asphalt-aggregates mixtures and tested at isothermal set temperatures of 40, 25, and 5°C [24].

Fracture toughness is an appropriate fracture resistances measure for linear-elastic isotropic- brittle materials. The HMA in this study does not meet these criteria. Despite these requirements, fracture toughness is still often employed to characterize the fracture resistance of HMAs [13-16, 23]. The AASHTO TP105 standard for “... determining the fracture energy of asphalt mixtures using the semi-circular bend geometry (SCB)” includes a section on fracture toughness yet has no provisions for the size independence (i.e. plane strain condition) of fracture toughness [23]. In this study, the plane-strain criterion from ASTM E399-12 is employed as follows

$$2.5 \left(\frac{K_{ic}}{\sigma_{ys}} \right)^2 \leq (W - a) \quad (4)$$

where K_{ic} is the approximate plane-strain fracture toughness, σ_{ys} is the yield strength, and $(W - a)$ is the initial ligament length. According to [Eq. (4)] and preliminary data, the current DCT specimen dimensions are inadequate to achieve the plane strain condition. Thus, according to ASTM E399-12, the fracture toughness recorded in this study hereon is defined as the “apparent” fracture toughness and reported everywhere with the thickness.

Another requirement for a valid K_{ic} is the elastic regime not exceed a certain degree of nonlinearity. For, the calculated K to bear relation to K_{ic} , the condition

$$P_{\max} / P_Q \leq 1.10 \quad (5)$$

must be true where P_{\max} is the maximum load during the test and P_Q is the intersect point of the 95% slope secant line starting at the initial nonlinearity of the force vs displacement curve. In the current study, the material meets this requirement at all temperatures.

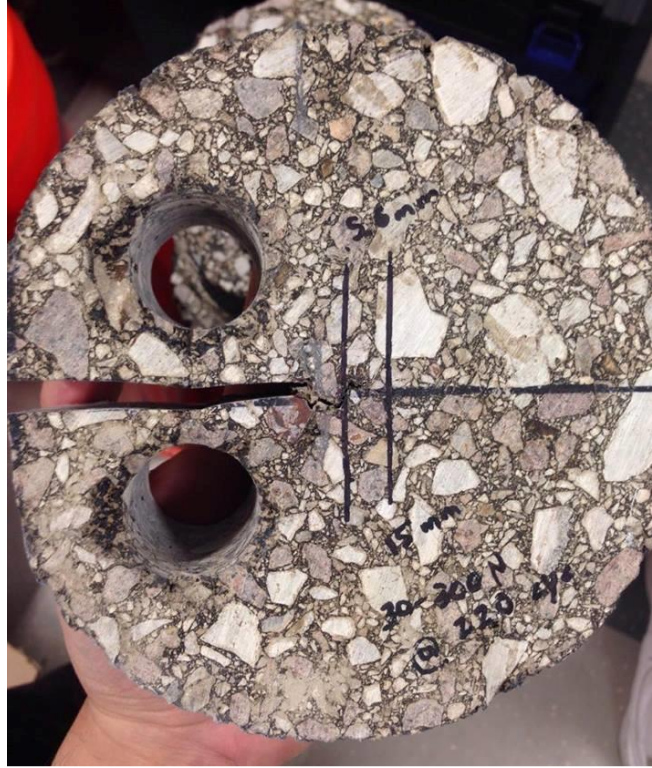


Figure 10 – Pre-cracked specimen according to 0.1B requirements

Pre-cracking is an important procedure that conditions (sharpens) the machined notch tip to simulate a “real” fully developed crack in a structure. Few such procedures have been developed for HMAs. A recent procedure for DENT specimen has been introduced in literature but to the authors knowledge it has yet to be codified [39]. In this study, the DCT specimens were subjected to fatigue pre-cracking per ASTM E647-15 [38]. The maximum stress intensity factor (in cycle), K_{\max} , during pre-cracking must not exceed 60% of the estimated plane-strain fracture toughness K_{ic} at a force ratio $R = P_{\min} / P_{\max}$ of 0.1. An estimate of K_{ic} and subsequently K_{\max} is calculated

using the results of the fracture energy tests. All stress intensity factors, K are calculated according to ASTM E399-12 as follows

$$K = \frac{P}{B\sqrt{W}} f\left(\frac{a}{W}\right) \quad (6)$$

where P is the load, B is the specimen thickness, W is the specimen width (depth), and the geometry factor $f(a/W)$ is calculated as

$$f\left(\frac{a}{w}\right) = \frac{\left(2 + \frac{a}{w}\right) \left[0.76 + 4.8 \frac{a}{w} - 11.58 \left(\frac{a}{W}\right)^2 + 11.43 \left(\frac{a}{W}\right)^3 - 4.08 \left(\frac{a}{W}\right)^4 \right]}{\left(1 - \frac{a}{W}\right)^{3/2}} \quad (7)$$

where a is the crack length as depicted in Figure 4b. According to ASTM E647-15, fatigue pre-cracking must continue until the crack has extended $a \geq 0.1B$ (≥ 5 mm) beyond the initial notch length. In this study, due to large aggregates, pre-cracking was performed until the crack grew by $a \approx 0.2B$ (approximately 10 mm) as depicted in Figure 10. The length of the pre-crack on the front and back surfaces must remain with $0.25B$ of each other. Additionally, the ASTM E647-15 standard requires that the crack not deviate from the plane of symmetry by more than $\pm 20^\circ$; however, due to the large aggregates this condition is not enforced.

Finally, the fracture toughness tests can be conducted at a constant rate. Here the ASTM E399-15 standard for metallic materials is not appropriate due to the extremely low strength of HMAs. Instead, the load rate applied in ASTM 7313-13 is applied at a constant crack mouth opening displacement (CMOD) of 0.017 mm/s. Before the K_{ic} calculation, validity requirement of $\frac{P_{\max}}{P_Q} \leq 1.10$ was established where P_{\max} is the maximum force during the test and P_Q is the

intersect point of the 95% slope secant line starting at the initial nonlinearity of the force vs

displacement curve. Type III of force-displacement (CMOD) records was expected from fracture energy test curves as seen in

Figure 11.

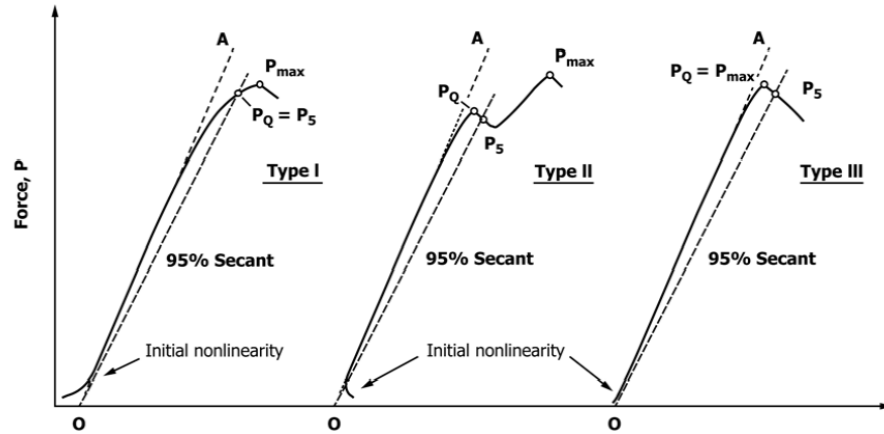


Figure 11 – Types of Force-Displacement Records [26].

It is important to note that the plane-strain condition has not been achieved for the DCT specimen of Type-C HMA in this study. The fracture toughness reported hereon is the “apparent” fracture toughness, K_c and is reported with respect to thickness.

The pre-cracking parameters including the maximum stress intensity, K_{max} , load range, ΔP , and stress intensity factor range, $\Delta K = (K_{max} - K_{min})$, for each temperature are listed in Table 3.

Table 3 – Pre-cracking parameters

Temperature, T (°C)	Maximum Stress Intensity, K_{max} (MPa \sqrt{m})	Load Range, ΔP (N)	Stress Intensity Range, ΔK (MPa \sqrt{m})
5	0.340	900	0.3060
25	0.085	225	0.0765
40	0.018	36	0.0162

Fatigue Crack Growth Rate Tests

Fatigue crack growth (FCG) tests were conducted following the ASTM E647-15 standard for the “... Measurement of Fatigue Crack Growth Rates” [38]. Since the true heterogeneous nature of HMA mixture, the most rigorous rules were adopted from the standard. The dimensions of the specimen were kept to ASTM 7313-13 [24]. Pre-cracking was carried out using the same procedure and parameters previously described. Fatigue precrack was determined from $0.1B$ (5 mm) to 10 mm. Both the pre-cracking and FCG tests were performed at the designated isothermal conditions after appropriate soak time. Cracking deviation on HMA mixtures occur at a wide range of $\pm\theta$ hence the requirement of $10^\circ < \theta \leq 20^\circ$ was not incorporated. Measurement of crack sizes on both front and back surfaces during pre-cracking required to be below $0.25B$.

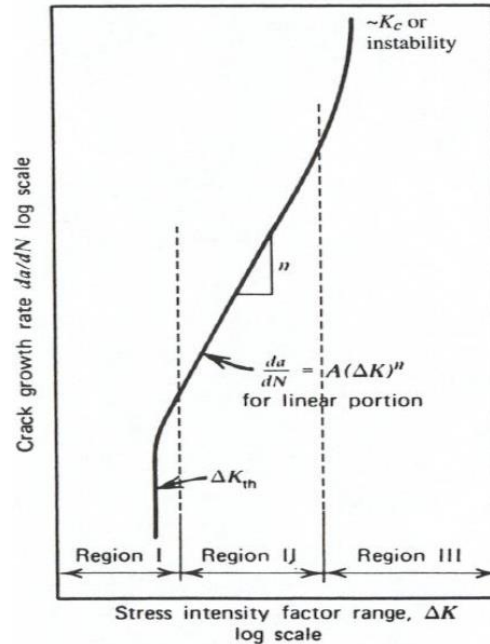


Figure 12 - Schematic sigmoidal behavior of fatigue crack growth versus ΔK .

Constant-Force-Amplitude procedure was employed at a stress ratio of $R=0.1$ and frequency of $f=0.1\text{Hz}$ with a triangular cyclic waveform. Crack growth measurements were done at every cycle using visual measurement. Images were taken with Vic-Snap and cracks were

measured using Image J software [37]. Pre-cracking and FCG tests were performed at 5, 25, and 40 °C.

The FCG test parameters for each temperature are listed in Table 4. The crack growth was measured using a digital image correlation system.

Table 4 – Fatigue crack growth test parameters

Temperature, T (°C)	Maximum Stress Intensity, K_{\max} (MPa $\sqrt{\text{m}}$)	Load Range, ΔP (N)	Stress Intensity Range, ΔK (MPa $\sqrt{\text{m}}$)
5	0.2700	720	0.2430
25	0.0315	90	0.0283
40	*NA	*NA	*NA

*NA – Not Applicable to be discussed later.

Chapter 4: Fracture Test Results At Different Thickness

ASTM Requirement

Preliminary experiments were performed to check the ASTM plane-strain condition [Eq.(1)]. Three indirect tensile tests (IDT) were performed recording an average yield strength, σ_{ys} of 849 kPa. Three DCT tests were performed at a specimen thickness of 50 mm measuring an average fracture toughness of $0.265 \text{ MPa}\sqrt{\text{m}}$. Taking these properties and evaluating [Eq.(1)], a specimen thickness of 244 mm or greater is required to achieve the plane-strain condition. To maintain a width-to-thickness ratio within the recommended range of $2 \leq W/B \leq 4$; the specimen width must be between $488 \text{ mm} \leq W \leq 976 \text{ mm}$. A specimen with the above dimensions is not practical to test and exceeds the typical thickness of laid HMA. In summary, for dense-graded HMA at 27°C, the fracture toughness measured using the standard DCT dimensions is the “apparent” fracture toughness, K_c and must be reported with specimen thickness.

Fracture Toughness

Fracture toughness tests were performed on triplicate specimens prepared at four thicknesses. The test results are presented in Table 5 with the load-displacement curves shown in Figure 13. On average, the peak load increases with thickness. At a given thickness, the peak load varies. The peak load variation is linked to the different initial notch length measured for each specimen after pre-cracking. The critical crack length at fracture is recorded and plotted with respect to the peak load in

Figure 14. Peak load versus critical crack length exhibits a linear relationship with a negative-slope. As the critical crack length increases the peak load decreases. The trend follows LEFM theory where when the fracture area decreases the force needed for fracture decreases. The dimensions, peak load, and critical crack length are applied to calculate the fracture toughness,

K_c . Fracture toughness is plotted against thickness Figure 15a. When compared to the LEFM theory in Figure 3, the HMA is in plane-stress at the given thicknesses. Theory states there exists a maximum fracture toughness in the transition from plane-stress to plane-strain. A quadratic function is fitted to the fracture toughness versus thickness data as follows $K_c(B) = -2.547\text{E-}05 \cdot B^2 + 4.485\text{E-}03 \cdot B + 9.807\text{E-}02$. Taking the derivative of the function and setting it equal to zero, the maximum fracture toughness is approximately $0.295 \text{ MPa}\sqrt{\text{m}}$ at a thickness of 88 mm. Using this approach, a design engineer can optimize the fracture resistance of HMA flexural pavement layers by optimal thickness depending on the COV. The COV of K_c is plotted versus thickness in Figure 15b. The COV is of acceptable magnitude for HMAs (below 15% acceptable, below 5% excellent) but is inconsistent at the given thicknesses with a drop at 40 mm that can be explained by the optimal air void % found in those specimens (7%). A high COV is expected in plane-stress since K_c is a local measure of fracture resistance while HMA is a heterogeneous.

In summary, for dense-graded HMA at 25°C, K_c depends on specimen thickness between 25 and 75 mm. The specimen is in plane-stress at $B \leq 88 \text{ mm}$ and plane-strain at $B \geq 244 \text{ mm}$. These findings are dependent on material, temperature, and specimen. Different HMA compositions and gradations will have different mechanical properties. The deformation and fracture mechanisms of HMAs change with temperature. Specimen that offer large fracture areas will produce lower COVs.

Table 5 – Fracture Toughness of Dense-Graded HMA

Specimen Name	Thickness B	Air Voids, AV	Critical Crack Length, a_c	Peak Load, P_c	Apparent Fracture Toughness, K_c	Avg.	Std. Dev.	COV
	(mm)	(%)	(mm)	(N)	(MPa√m)	(MPa√m)	(MPa√m)	(%)
K25-1	26.5	6.9	37.1	236.5	0.171	0.197	±0.035	17.5
K25-2	27.0	6.3	43.0	223.6	0.184			
K25-3	25.1	6.4	54.5	190.4	0.236			
K40-1	41.4	7.1	39.2	463.7	0.228	0.235	±0.014	6.0
K40-2	39.9	7.1	44.0	377.7	0.227			
K40-3	41.2	7.1	54.9	332.5	0.252			
K50-1	50.4	6.8	38.5	678.3	0.277	0.265	±0.029	11.1
K50-2	57.8	6.3	40.3	645.5	0.232			
K50-3	48.9	7.5	47.8	548.4	0.288			
K75-1	73.2	7.3	47.8	695.8	0.248	0.289	±0.035	12.2
K75-2	73.4	6.6	59.2	625.3	0.307			
K75-3	73.6	6.8	71.1	393.7	0.311			

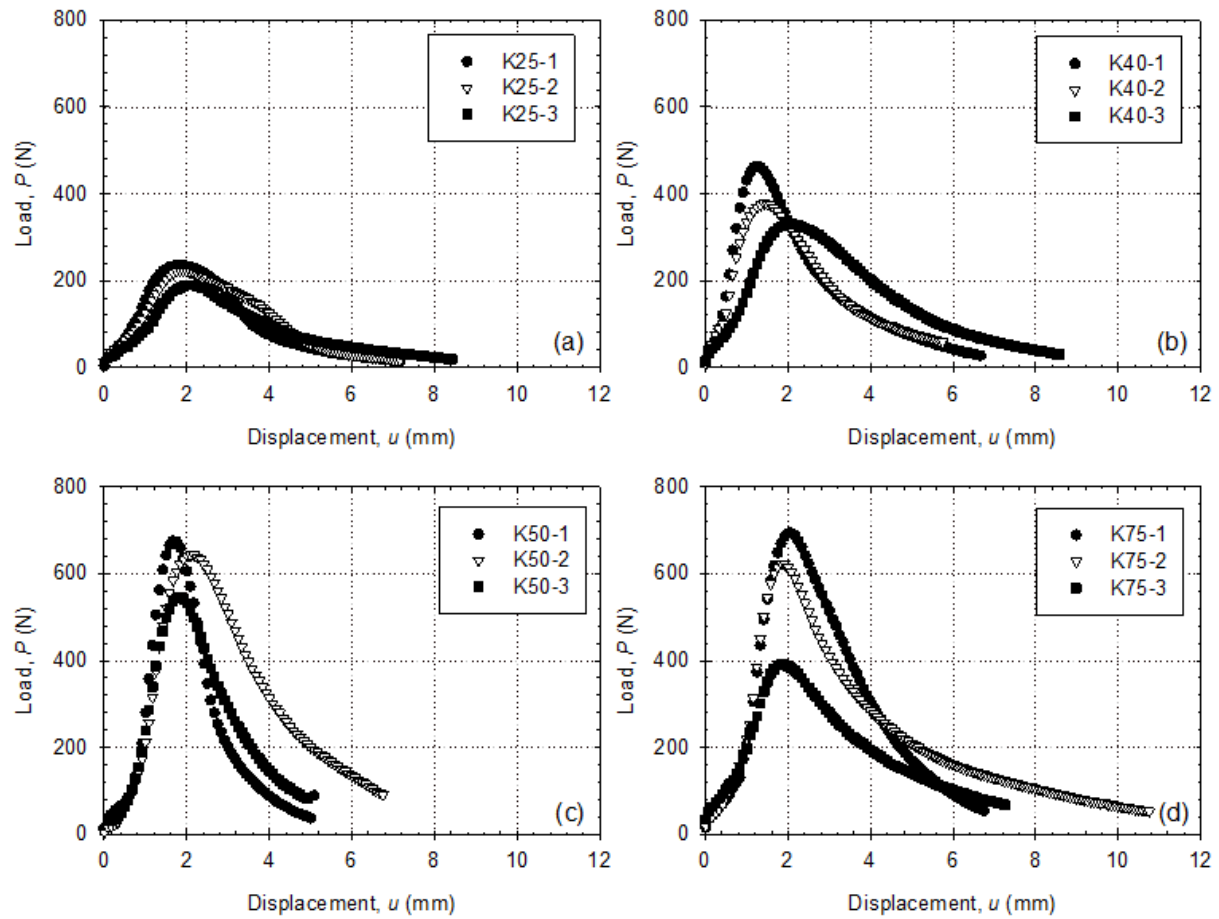


Figure 13 – Load-displacement curves of fracture toughness tests at thicknesses from (a) 25 to (d) 75 mm respectively

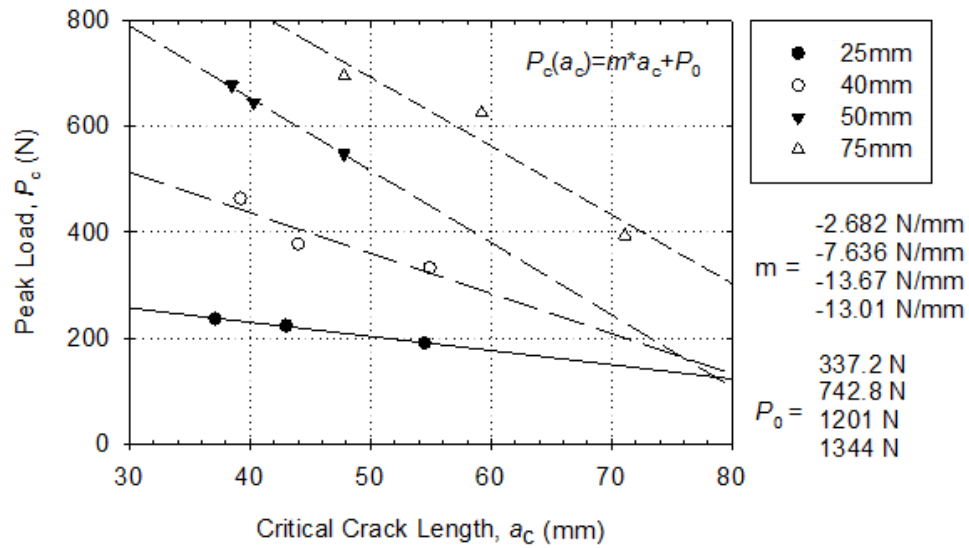


Figure 14 – Peak load versus critical crack length

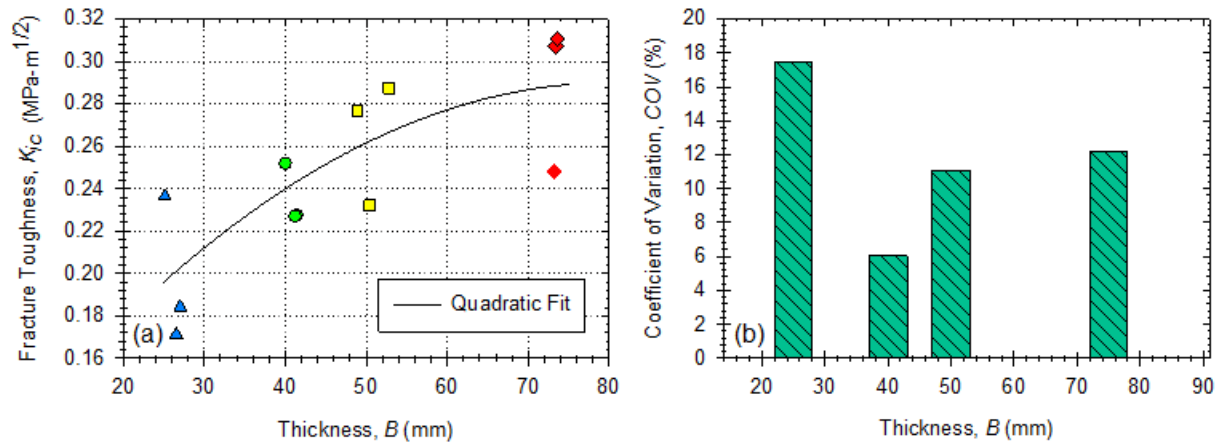


Figure 15 – Fracture toughness versus thickness: (a) magnitude and (b) coefficient of variation
Fracture Energy

Fracture energy tests were performed on triplicate specimens at four different thicknesses. The test results are presented in Table 6 with the load-displacement curves shown in Figure 16. The fracture energy load-displacement curves have a tight grouping when compared to the fracture toughness tests in Figure 13. At a given thickness, the peak load remains relatively constant. This trend relates to the absence of pre-cracking. On average, the peak load and work of fracture increase with thickness. The initial dimensions and work of fracture are applied to calculate the fracture energy, G_f . Fracture energy is plotted against thickness in Figure 17a. On average, fracture energy remains constant at thicknesses between 25 to 75 mm. The COV of G_f is plotted versus thickness in Figure 17b. The COV of G_f is thickness-dependent and decreases as the thickness increases from a COV of 23.4% at 25 mm to 3.3% at 75 mm. The standard 50 mm thickness (recommended by ASTM D7313-13) is sufficient to obtain consistent fracture energy measurements at a COV of 3.1%.

In summary, for dense-graded HMA at 25°C, G_f is not dependent on specimen thickness between 25 and 75 mm while the COV is dependent on specimen thickness. Similar to fracture

toughness, these findings are dependent on material, temperature, and specimen. For example, Wagoner et al. [9] found specimen size has a significant impact on the fracture energy of a 9.5 mm max aggregate mixture with PG 64-22 asphalt binder at -10°C. Overall, the fracture toughness and energy of a given HMA mixture must be evaluated experimentally at the expected service conditions (layer thicknesses, temperature range, strain rates) before any conclusions concerning the dependencies of a given mixture can be made.

Table 6 – Fracture Energy of Dense-Graded HMA

Specimen Name	Thickness, B	Air Voids, AV	Ligament Length, $W - a$	Work of Fracture, W_f	Fracture Energy, G_f	Avg.	Std. Dev.	COV
	(mm)	(%)	(mm)	(J)	(J·m ⁻²)	(J·m ⁻²)	(J·m ⁻²)	(%)
G25-1	26.9	6.8	83.9	1.265	560.7			
G25-2	27.1	6.1	77.8	1.457	691.2	714.7	±167.1	23.38
G25-3	25.2	6.3	81.6	1.835	892.4			
G40-1	41.5	7.5	81.3	2.634	780.6			
G40-2	41.8	7.0	79.8	2.141	642.0	718.2	±70.32	9.791
G40-3	42.3	7.3	82.5	2.555	732.0			
G50-1	53.1	6.4	82.3	2.915	667.2			
G50-2	53.0	6.9	79.4	2.700	641.8	645.6	±19.98	3.095
G50-3	54.7	6.8	82.4	2.830	627.8			
G75-1	74.7	7.5	81.5	4.153	682.1			
G75-2	75.0	7.5	80.5	4.186	693.1	700.8	±23.44	3.345
G75-3	76.0	7.9	82.3	4.548	727.1			

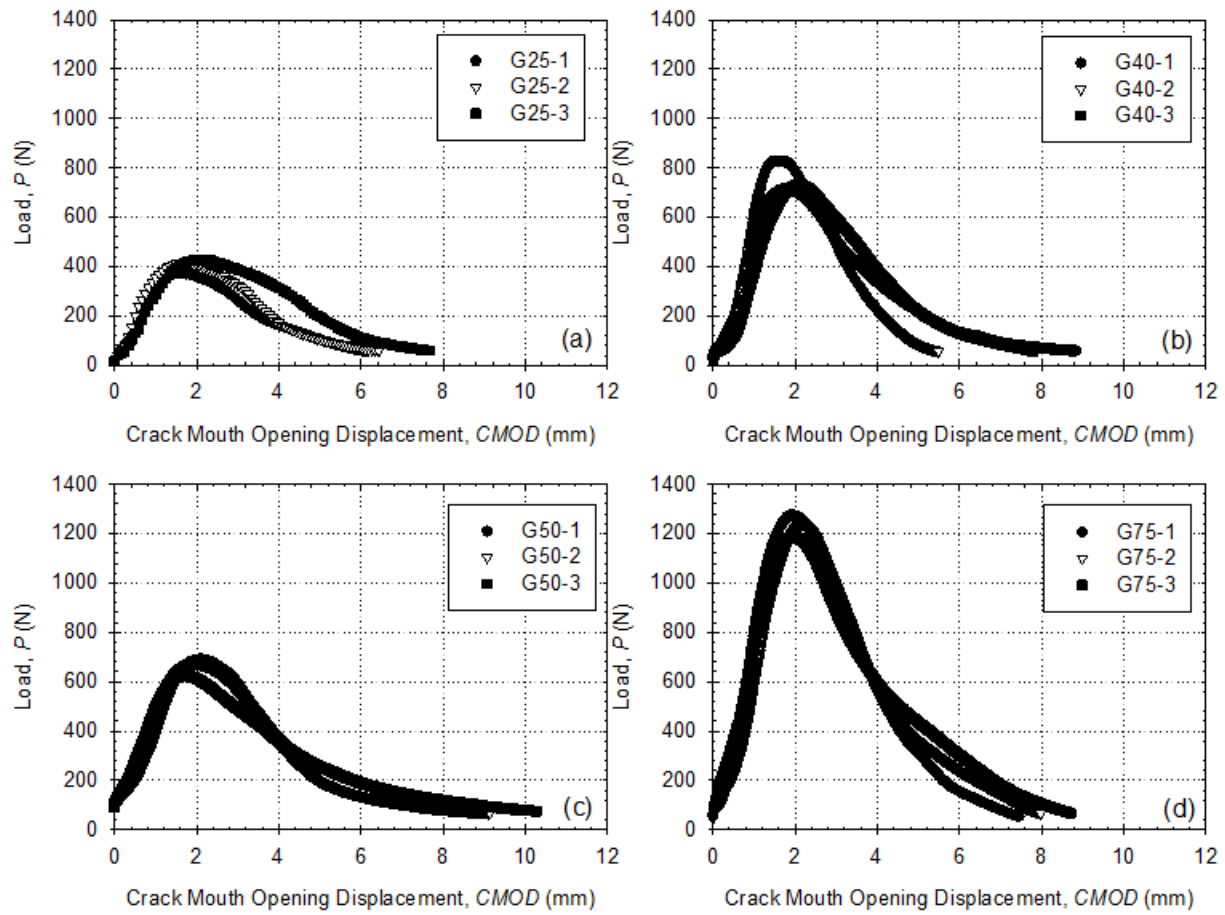


Figure 16 – Load-CMOD curves of fracture energy tests at thicknesses from (a) 25 to (d) 75 mm respectively

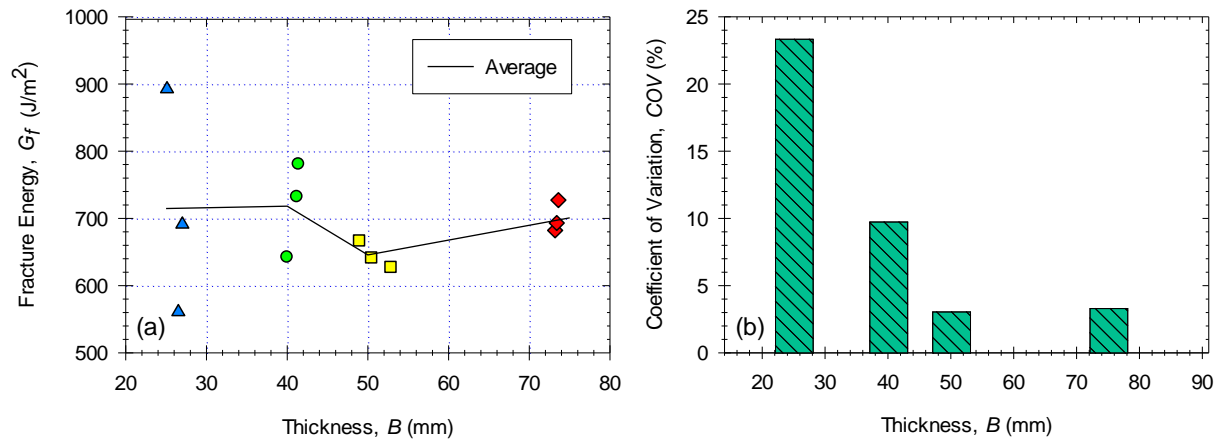


Figure 17 – Fracture energy versus thickness: (a) magnitude and (b) coefficient of variation

Crack Path

Photographs of the crack path for each K_c and G_f specimen are presented in Figure 18 and Figure 19, respectively. In both tests and at all thicknesses, the primary crack propagates through the bitumen bypassing most large aggregates. From specimen-to-specimen, the crack is torturous and travels uniquely through the heterogeneous structure following a path of least resistance. In limited cases, the crack bisects moderately sized aggregates. These failed aggregates are primarily found at long cracks near the points where the specimen separated in half. In summary, for dense-graded HMA at 25°C, there is no trend between crack path and thickness.

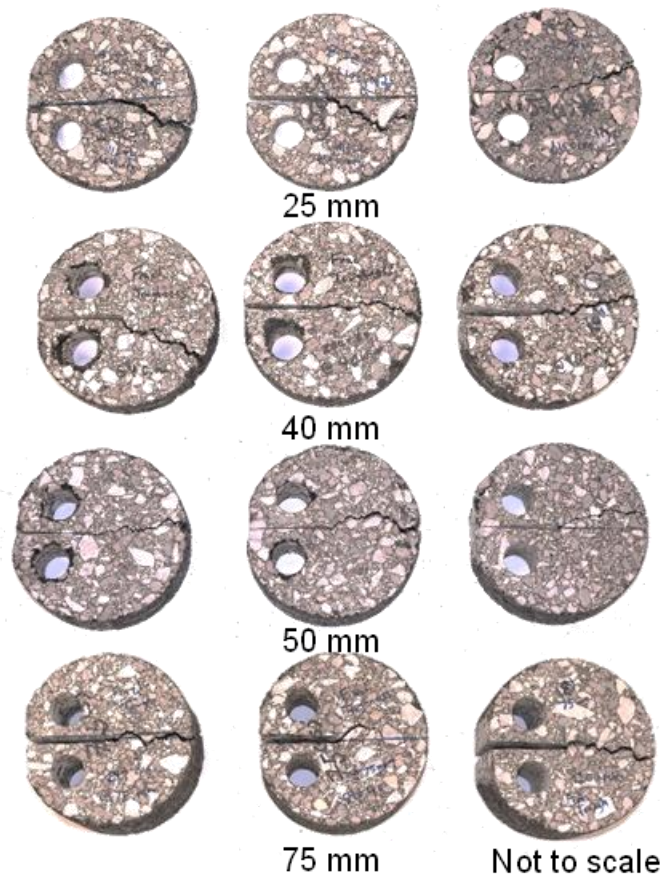


Figure 18 – Crack Path observed in K_c specimen

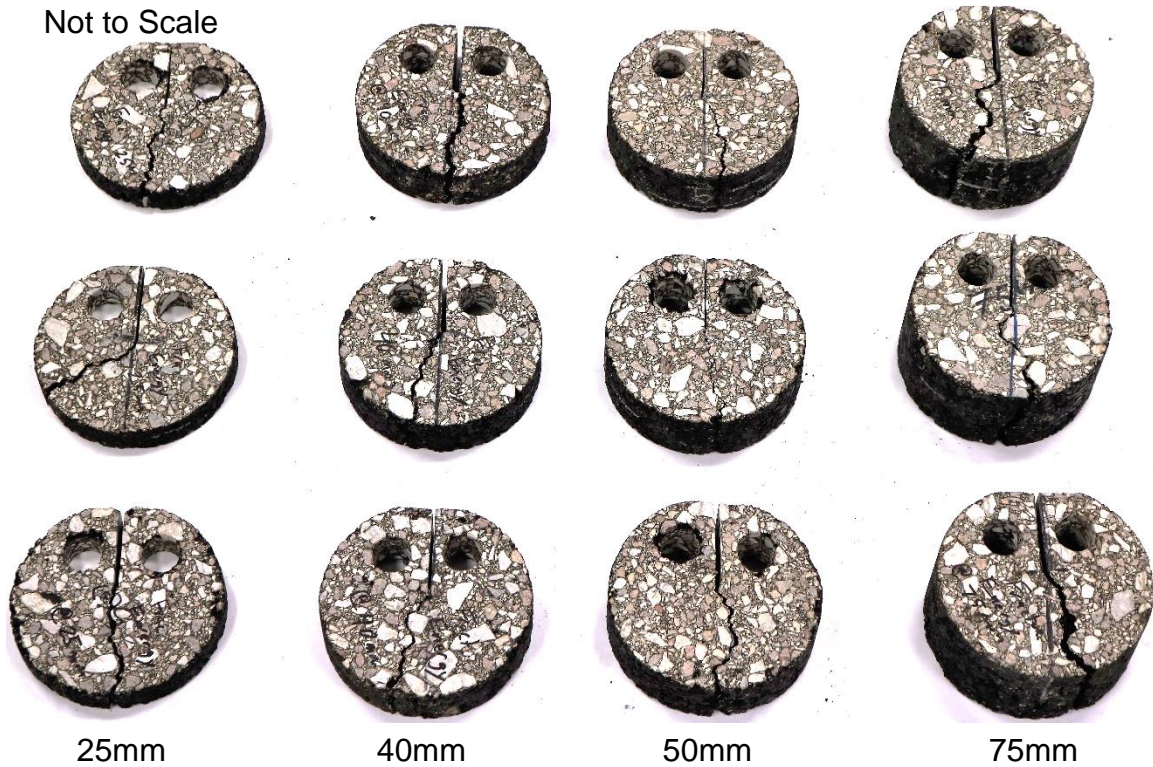


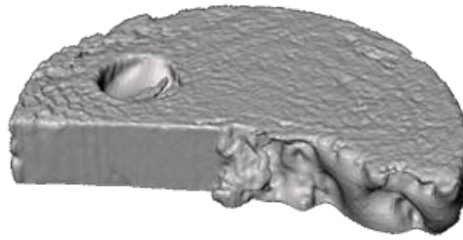
Figure 19 – Crack Path observed in G_f specimen

3D Surface Scanning

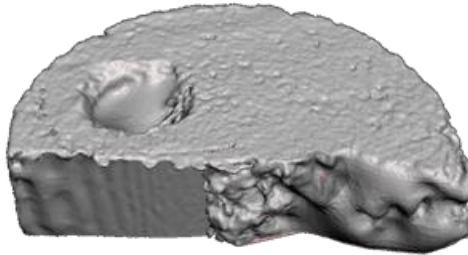
In homogeneous linear-elastic materials, the fracture surface should evolve with thickness as illustrated in Figure 3. Under plane-stress, a slant crack should be observed. In the transition from plane-stress to plane-strain a mixed-mode fracture surface, including both shear lips and a flat surface, should be observed. In plane-strain, the fracture surface should be flat with minimal shear lips.

3D surface scans taken of G_f specimens at different thicknesses are shown in Figure 20. The trends for homogenous linear-elastic materials do not hold for dense-graded HMA. It was previously determined that dense-graded HMA is in plane stress when $B \leq 88$ mm and plane-strain when $B \geq 244$ mm. Examining the 3D scans, the fracture surfaces at all thicknesses are non-planar and reside between 0 and 45°. The crack bypasses aggregates leading to a tortuous and

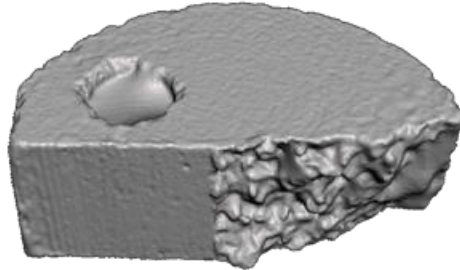
cratered fracture surface. It is possible that the crack may become more planar as the specimen approaches plane-strain, $B \geq 244$ mm ; however, the gradation chart for the dense-graded mix used (Table 1) suggests the fracture surface can remain out-of-plane by up to 19 mm (the largest aggregates size). In summary, for dense-graded HMA at 27°C, 3D scans of the fracture surface cannot reasonable predict the plane-stress or plane-strain condition.



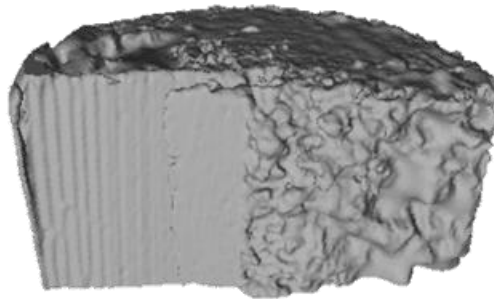
25mm



40 mm



50 mm



75 mm

Note: Not to scale

Figure 20 – 3D Fracture Surface at specimen thicknesses from 25 to 75 mm

Chapter 5: Fracture And Fatigue Crack Growth Results At Different Temperatures

The tensile and fracture properties of the mixture listed in Table 7 were obtained following the ASTM D7313-13, E399-12 and E647-15 test standards respectively [24,26,38]. The summarized test results shown are the average values of three specimens tested for each temperature and testing method. From these results, it can be observed that throughout all tests the properties increased at low temperatures and decrease at high temperatures. Strength increased by 240% and decreased by 64% with respect to 25 °C. Fracture energy increased by 32% and decreased by 78%. Fracture toughness increased by 167% and decreased by 79%. As a result of thermoplastic behavior within the material, the lower the temperature the more difference in properties is observed.

Table 7 – Tensile and Fracture Properties of HMA Type-C

Temperature, T °C	Indirect Tensile Strength, σ_{UTS} MPa	Fracture Toughness, K_{Ic} ($MPa\sqrt{m}$)	Fracture Energy, G_f ($J\cdot m^{-2}$)
5	2889.52±122.84	0.7099±0.074	957.10±259.44
25	849.15±30.98	0.2654±0.029	645.60±19.98
45	302.73±19.00	0.0534±0.010	135.58±16.54

Indirect Tensile Strength

The indirect tensile tests results are summarized in Table 8 and strength curves for the different temperatures are shown in Figure 21. Indirect tensile specimens were precondition overnight (~8 hrs) and 4 hours for tests at 5 and 40 °C respectively. Tests at high temperature exhibit the highest axial displacement up to 13.7 mm and plastic behavior after reaching peak loads. Low temperature results show a linear elastic region and brittle fracture characterized in bituminous mixtures at these temperatures where low plastic deformation is observed and damage is concentrated leading to rapid crack susceptibility. Strength drastically increased at 5 °C while at 40 °C the increase in

temperature resulted in major deformation susceptibility and low strength with respect to room temperature. Coefficient of variation was slightly higher for high temperature due to the higher molecular mobility and viscous response however all values were within a good COV.

Table 8 – Indirect tensile strength properties

Specimen No.	Temperature, T (°C)	Air Voids, AV (%)	Max. Load, P_{max} (kN)	IDT Strength, S_t (KPa)	Avg. (KPa)	Std. Dev. (KPa)	COV (%)
IDT5-1	5	6.8	35.28	2805.36	2889.52	±122.84	4.25
IDT5-2		7.5	35.63	2832.71			
IDT5-3		7.2	38.11	3030.49			
IDT25-1	25	7.9	10.99	850.59	849.15	±30.98	3.65
IDT25-2		6.6	11.06	879.45			
IDT25-3		7.8	10.29	817.48			
IDT40-1	40	7.6	3.81	303.21	302.73	±19.00	6.28
IDT40-2		7.0	3.56	283.58			
IDT40-3		6.5	4.04	321.53			

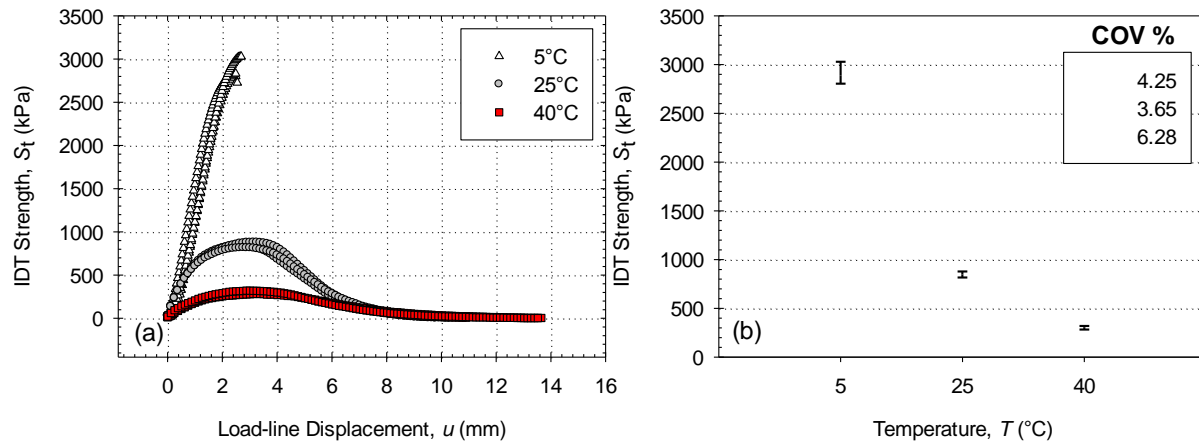


Figure 21 - IDT (a) strength-displacement curves and (b) strength with COV

Fracture Energy Results

The fracture energy test results are summarized in Table 9 and graph curves are shown in Figure 22. The load-displacement curves of the fracture energy tests are like those of the IDT tests with a brittle high-strength material at 5°C that relaxes into an extremely ductile low-strength material at 40°C. Difference in fracture energy is more noticeable at elevated temperature. At 5°C,

fracture energy increased by 48% with respect to room temperature with an average of 957.10 J/m². It did not increase much due to the low CMOD and energy dissipation upon fracture. The work done by the load was mainly stored as elastic strain energy prior to the brittle fracture and neglecting the viscous dissipation of the material. At 25°C, the fracture energy was 645.60 J/m² with an average maximum load and CMOD of 0.663 kN and 12 mm respectively. At 40°C, fracture energy decreased by 79% with respect to room temperature with an average of 135.58 J/m². Specimens exhibit the largest CMOD and lowest peak load, resulting in the lowest area under the load-CMOD curve.

The COVs obtained from fracture energy tests at 5, 25, and 40°C are 27.11, 3.095, and 12.20% respectively. A large coefficient of variation is observed for the 5 °C temperature which can possibly be attributed to a variation in the microstructure of the specimen coupled with the embrittlement of the binder contributing to an inconsistent load-CMOD curve. The low temperature caused the binder to become brittle leading to a rapid crack at the elastic region and lesser energy dissipation decreasing fracture energy in that specimen [16]. The COV at 5 °C is still however, within the expected ranges for asphalt mixture testing. Coefficient of variation obtained from fracture energy results are reasonably good for 25 and 40 °C.

Different fracture mechanisms were observed at each temperature. At 5°C, upon crack propagation, it was noticed that the crack tended to grow through both the aggregates and the mastic. At 25°C, the crack was mixed with propagation around the aggregates and through them. At 40°C the crack mostly propagated around the aggregates. Secondary cracking was prominent at 40°C due to a large plastic zone. Temperature can greatly influence the binder and aggregate interface, a rigid network within the material is produced at low temperatures limiting molecular mobility whereas at high temperature the binder allows a crack path of least resistance [28].

Table 9 – Fracture energy properties

Specimen No.	Temperature, T	Air Voids, AV	Max. Load, P_{max}	Fracture Energy, G_f	Avg.	Std. Dev.	COV
	(°C)	(%)	(kN)	(J/m ²)	(J/m ²)	(J/m ²)	(%)
G5-1	5	7.1	1.946	989.86	957.10	±259.44	27.11
G5-2		7.3	1.480	682.83			
G5-3		7.1	2.730	1198.61			
G25-1	25	6.9	0.676	641.84	645.60	±19.98	3.10
G25-2		6.8	0.624	627.77			
G25-3		6.4	0.690	667.20			
G40-1	40	7.3	0.083	146.33	135.58	±16.54	12.21
G40-2		7.0	0.080	143.88			
G40-3		6.3	0.113	116.52			

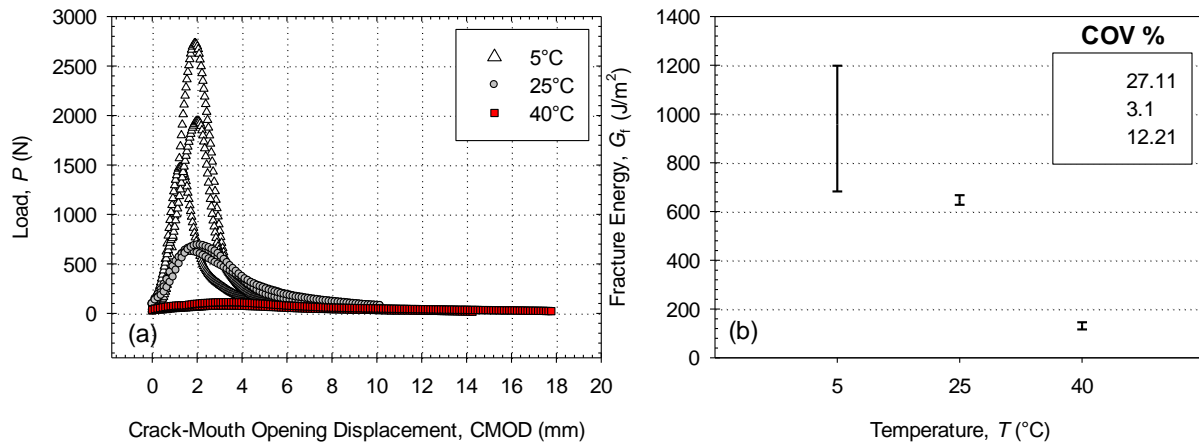


Figure 22 - Fracture energy (a) load-CMOD curves and (b) strength with COV

Fracture Toughness

The fracture toughness test results are summarized in Table 10 with the Load-CMOD and fracture toughness-temperature graphs shown in Figure 23. Again, the load-CMOD curves of the fracture toughness tests are similar to both the IDT and fracture energy curves. Unlike the previous two tests, the fracture toughness specimens were pre-cracked and therefore each specimen had a different initial notch length. As explained above, the fracture toughness tests were precracked at a K less than 60% of K_{ic} estimated. The estimated K_{ic} calculated, according to the fracture energy peak loads results, were 0.250, 0.060, and 0.680 MPa√m for 25, 40, and 5 °C respectively. These

estimations were calculated including a pre-cracking size of $0.1B$ (5 mm) and dimensions (work ligament area, crack length, and thickness) measured in each specimen. The current DCT fracture test assumes the machined notch already as the pre-cracking requirement but this narrow crack does not account for a sharp crack tip [9]. This fundamental procedure aspect has been addressed only by sliding a fresh razor blade in *Zofka*. and *Edwards* study [39, 40], while other studies assume pre-cracking along with the initial crack [9,12,16].

The COV values demonstrated an increase as temperature increase. At 5°C, the lowest COV was found due to the small process zone and less branching of the crack. At 25 °C, the COV increased by 0.51% as the fracture process zone increased. At 40 °C, the largest fracture toughness COV was produced due to the wide fracture process zone (FPZ) and the bridging zone ahead of the crack tip [2]. The calculated K_{ic} vs the average K_q from the test results were similar considering the difficulty on measuring the crack. Determination of the notch lengths indicated the largest values at 40 °C while the lowest values were measured at 25 °C.

Fracture toughness increased by 167% at 5 °C with respect to room temperature while at 40 °C this value dropped by 80% as shown in Figure 23. The evolution and increase of fracture toughness with respect to temperature is depicted in Figure 24. Considering *Aliha et al.* recent study [41], the stress intensity factor calculated in a modified bitumen material with the same binder performance grade as the current study was $1.2 \text{ MPa}\sqrt{\text{m}}$ at -15 °C. Looking at the behavior predicted in Figure 24, a trend increasing to that value can be estimated at – 15 °C. Another recent study from *Stewart* [11], shows a fracture toughness of a SP-D HMA with the same asphalt and binder PG listed in Table 2 of $0.287 \text{ MPa}\sqrt{\text{m}}$ at 25 °C. Both of these studies calculated the fracture toughness using SCB test procedures. The fracture toughness results obtained with the proposed DCT method can be assumed as reliable and within fidelity of results found in literature review.

In summary, both fracture energy and fracture toughness tests demonstrated similar fracture mechanisms. The results obtained with the proposed DCT method generated repetitive results and overall low COVs. A decrease in fracture energy and fracture toughness is seen as temperature increases. An increasing COV trend can be observed as temperature increases, with the exception of specimen G5-2 seen in Table 9 which produced inconsistent average and COV values. At 5 °C, damage within the specimens was concentrated and brittle fracture was observed. At 25 °C, the structure behaved as a visco-elastic material with crack and deformation susceptibility. At 40 °C, the material behaved in a viscous manner allowing for large plastic deformation and bifurcation of the primary crack.

Table 10 – Fracture toughness properties

Specimen No.	Temperature, T	Air Voids, AV	Notch Length, a	Fracture Toughness, K_{Ic}	Avg.	Std. Dev.	COV
	(°C)	(%)	(mm)	(MPa \sqrt{m})	(MPa \sqrt{m})	(MPa \sqrt{m})	(%)
K5-1	5	7.2	46.88	0.777	0.709	± 0.074	10.56
K5-2		6.9	43.75	0.722			
K5-3		6.9	48.97	0.629			
K25-1	25	7.3	38.47	0.232	0.265	± 0.029	11.07
K25-2		6.8	40.30	0.287			
K25-3		6.4	47.77	0.276			
K40-1	40	6.3	39.21	0.045	0.053	± 0.010	20.54
K40-2		7.4	52.72	0.065			
K40-3		7.5	50.82	0.049			

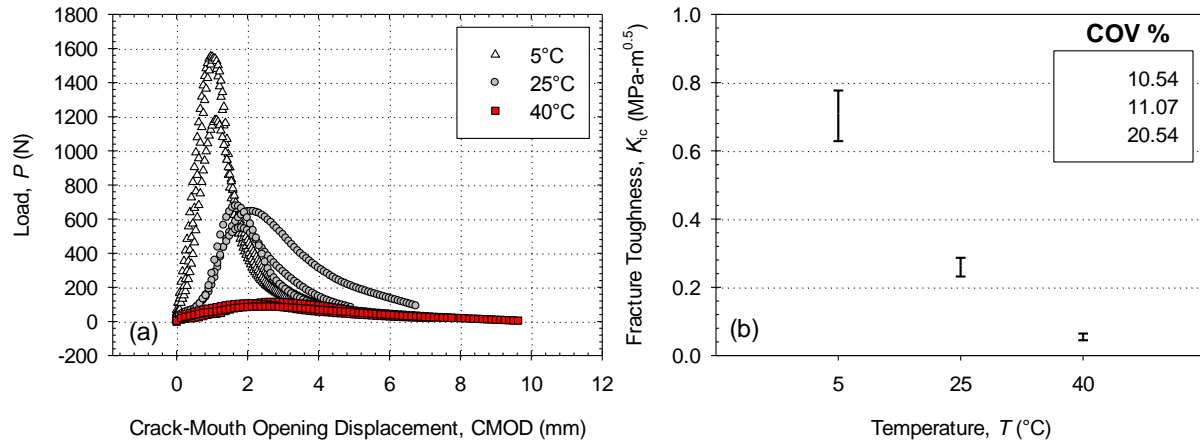


Figure 23 - Fracture toughness (a) load-CMOD curves and (b) strength with COV

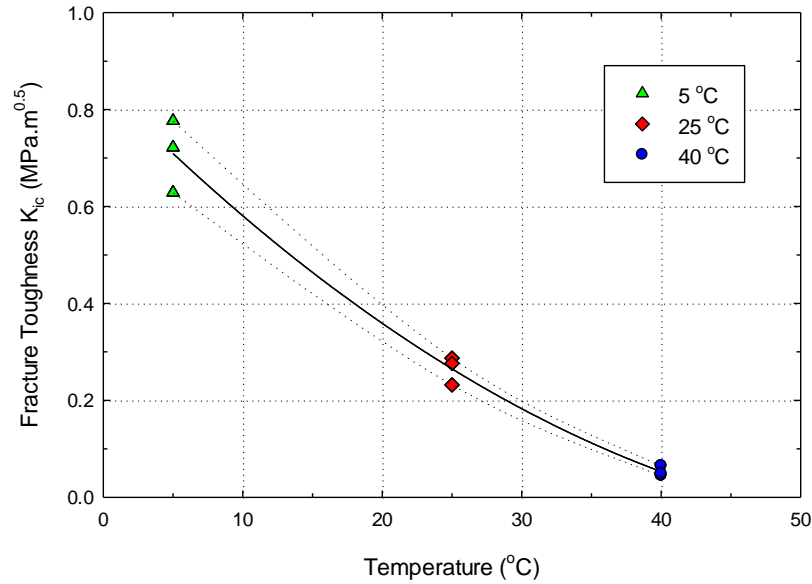


Figure 24 - Fracture toughness behavior at different temperatures.

Taking IDT and fracture toughness properties in Table 8 and Table 10 and evaluating [Eq.(1)], a specimen thickness of $B \geq 151\text{mm}$ and $B \geq 77\text{ mm}$ is required to achieve the plane-strain condition at temperatures 5°C and 40°C respectively. To maintain a width-to-thickness ratio within the recommended range of $2 \leq W/B \leq 4$; the specimens' width must be between $301\text{mm} \leq W \leq 602\text{mm}$ and $153\text{mm} \leq W \leq 307\text{mm}$ for 5°C and 40°C respectively. A specimen with

the above dimensions is not practical to test and exceeds the typical thickness of laid HMA. In summary, for dense-graded HMA at 5°C and 40°C, the fracture toughness measured using the standard DCT dimensions is the “apparent” fracture toughness, K_c and must be reported with specimen thickness.

Fatigue Crack Growth

Three samples were tested at each temperature and the fatigue crack growth results were plotted as stress intensity factor (SIF) vs crack growth. However, at high temperatures asphalt mixtures become highly susceptible to deformation and behave in a viscous manner. At these temperatures, bituminous mixtures turn into viscous fluids instead of elastic solids due to the sliding of molecular network. At 40°C, the primary crack did not form at the notch tip, instead appearing at the loading holes as depicted in Figure 25. At elevated temperature, the viscosity of the binder decreases leading to gross plasticity and an inability to successfully redistribute stress. The weakened matrix contributes to micro-damage zones throughout the specimen [28]. As a result, the FCG tests could not be successfully performed for dense-graded HMA (Type-C) in the DCT configuration at 40°C. Large scale yielding is characterized as the extensive plasticity affecting and increasing the yield zone making the parameters geometry dependent and highly variant. Disk shape compact tension method for FCG may not be reliable at high temperatures, also rutting becomes the main concern of distress in asphalt mixtures at these temperatures. These problems did not occur during the 5 and 25°C FCG tests.

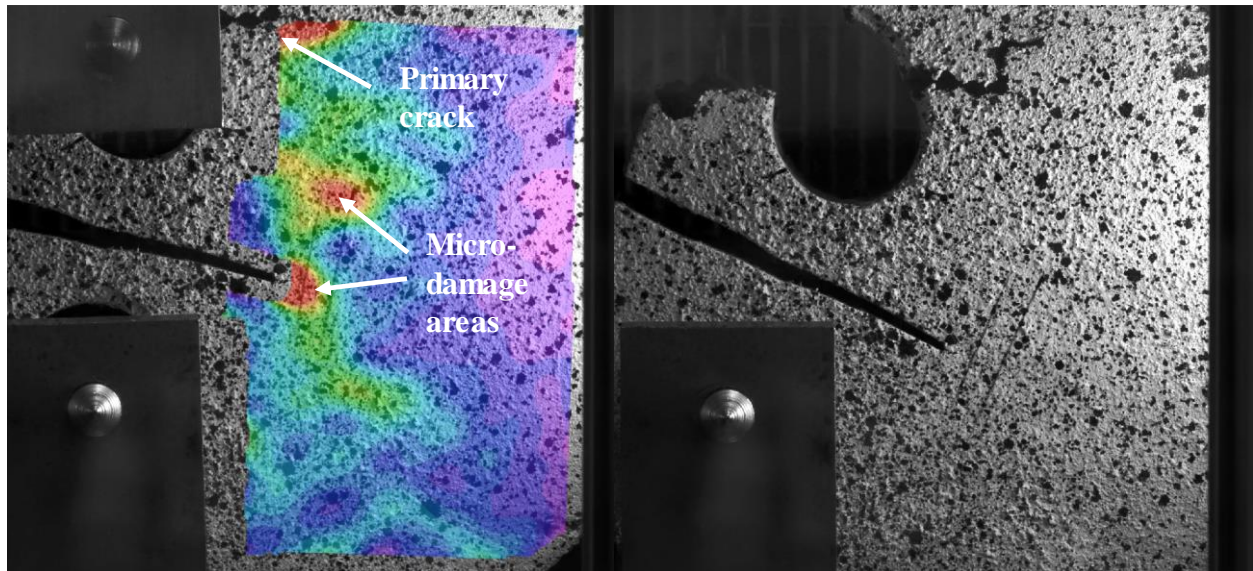


Figure 25 - Early failure at the loading grips for the 40 °C fatigue crack growth tests.

Table 11– Fatigue crack growth test conditions

Specimen No.	Air Voids, AV	Temperature, T	Loading Range, ΔP	Stress Intensity Range, ΔK	Initial Notch Length, a	Cycles to Failure, N_f
	(%)	(°C)	(N)	(MPa $\sqrt{\text{m}}$)	(mm)	(cycles)
F5-1	6.8	5	720	0.2430	31.97	371
F5-2	7.6				34.70	457
F5-3	6.7				29.28	404
F25-1	6.7	25	90	0.0283	33.33	2840
F25-2	7.2				35.15	2300
F25-3	7.5				28.32	2330
F40-1	NA	40	NA	NA	NA	NA
F40-2						
F40-3						

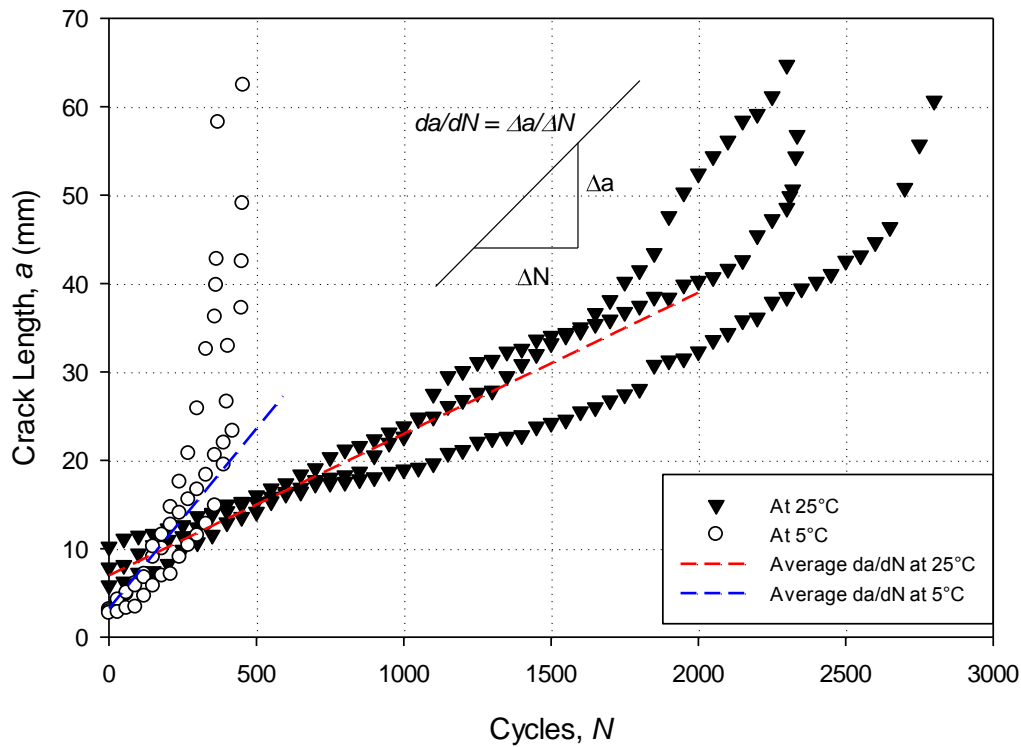


Figure 26 – Fatigue crack length versus cycles at each temperature

The FCG tests are performed under load-control at a stress ratio $R=0.1$. The tests conditions are listed in Table 11. The fatigue crack length including pre-cracking length versus cycles at each temperature is plotted in Figure 26. Initial average crack length was 30.28 mm for both temperatures. At 25 °C, an increase in crack growth rate is observed after 2000 cycles. Crack growth, however, was unstable during fatigue life as seen in the specimens at 25°C in Figure 26. Crack growth rate varied at some portions of the plot. This trend relates to the cracking propagation following least resistance paths through the binder and around the aggregates. The average fatigue crack growth rate is calculated before rapid crack growth rate (2000 cycles) as 0.016 mm/cycle. At 5 °C, the ΔK range was increased due to the excessive extent of testing time. The cooling chamber could only maintain temperature for a time period therefore the specimens failed at a reduced number of cycles. An increase in crack growth rate is observed after 350 cycles. The crack

growth rate curve looks smoother before crack length increase due to the brittleness within the structure and elastic solid behavior. The average fatigue crack growth rate is calculated before rapid crack growth rate (350 cycles) as 0.0407 mm/cycle.

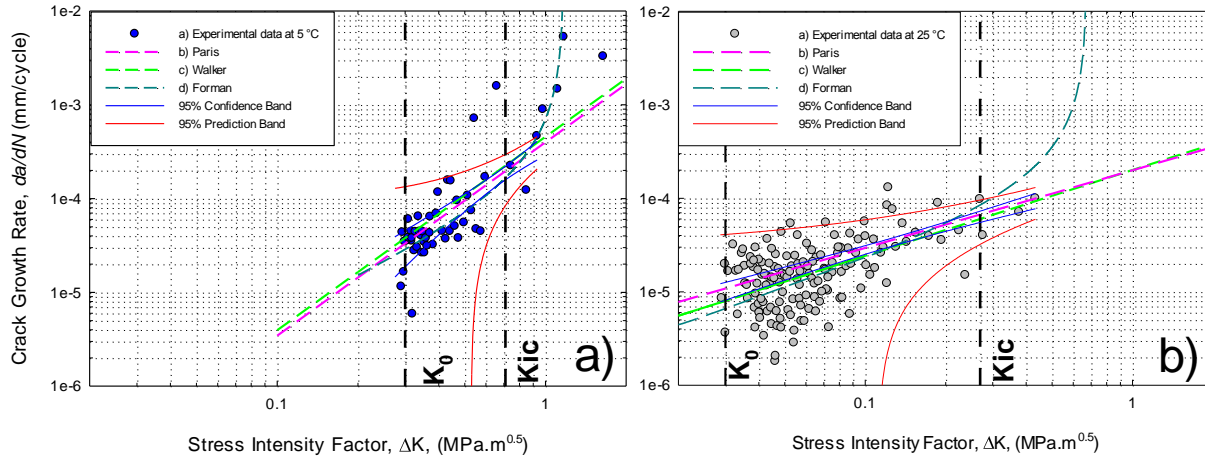


Figure 27 - Fatigue crack growth rate versus stress intensity range at (a) 5 and (b) 25 °C

The fatigue crack growth rate is plotted with respect to stress intensity factor range in Figure 27. The da/dN data is scattered. It is worth noting that K_0 is not equal to K_{th} , K_0 is just the lower SIF calculated from the data at the start of these tests. The scatter decreases as the specimens' approach the average fracture toughness. This scatter is due to torturous cracking where the crack encounters obstacles (hard aggregates) and/or soft regions (voids, unbonded interfaces etc.) that cause the crack growth rate to locally decrease and/or increase. This type of scatter can be explained by the inhomogeneity of the material, and is also seen in *Tschegg* study where the FCG behavior of asphalt BTI/16 produce large scatters ranging from $1\text{E-}7$ to $2\text{E-}6$ at 10°C [2]. Comparing the curves, it is observed that crack growth rates at 5°C are ten to a hundred times faster than 25°C . Near the fracture toughness, the crack growth rates were $1.7\text{E-}4$ and $7.0\text{E-}5$ mm/cycle at 5 and 25°C respectively.

Table 12– Model constants

Temperature, T (°C)	Average Fracture Toughness, K_{Ic} (MPa√m)	Paris		Walker		Forman		
		C	m	C	γ	C'	m'	K_c (MPa√m)
5	0.709	4E-4	2.062	4.58E-4	0.380	1.2E-4	1.30	1.30
25	0.269	2E-4	0.830	2.02E-4	1.082	1.2E-4	0.95	0.75

The crack growth rate, da/dN is plotted against the stress intensity factor range, ΔK on a log-log scale where ΔK is calculated using [Eq. (6)]. In this study, three laws are applied to model the fatigue crack growth behavior. The Paris law is applied as follows

$$\frac{da}{dN} = C(\Delta K)^m \quad (8)$$

where da/dN is the crack growth per cycle (mm/cycle), ΔK is the stress intensity factor range, and C and m are material constants. Paris law is capable of modeling only region II of the FCG-curve. The Walker law is written as follows

$$\frac{da}{dN} = \frac{C(\Delta K)^m}{(1-R)^{m(1-\gamma)}} \quad (9)$$

where C and m are the Paris material constants, γ is a material constant, and R is the stress ratio. The Walker law is capable of modeling region II of the FCG-curve and describes the mean stress effect. Finally, the Forman's law is described as follows

$$\frac{da}{dN} = \frac{C'(\Delta K)^{m'}}{(1-R)(K_c - K_{\max})} \quad (10)$$

where C' and m' are not the Paris material constants, K_{\max} is the maximum stress intensity factor during a cycle, and K_c is the apparent fracture toughness. The Forman law is capable of modeling both region II and III of the FCG-curve and describes the mean stress effect.

The Paris, Walker, and Forman laws are fit to the da/dN data as shown in Figure 27. The calibrated material constants for each model are listed in Table 12. A power curve fit is performed with confidence and prediction bands through the linear region of the data between K_0 and K_{ic} . The Paris and Walker models fitted most of the data for both temperatures. Although the slight difference, the Paris law and Walker model predictions lie within the confidence bands of the experimental data and fully inside the 95% prediction bands fitting most of the data even towards fracture, both Paris and Walker can be considered optimal models at this temperature. For the 25 °C tests, Walker model shows a slightly more conservative behavior through the data at low SIF values and the slope better describes the FCG life prediction as ΔK increases. The Forman law is able to model region II and region III of the FCG curve at 5 °C by modifying the fracture toughness to 1.30 MPa \sqrt{m} . As the Forman model incorporates material constants C' and m' (empirical FCG constants not known for this material), this model overpredicts the unstable crack region at 25 °C. This material does not demonstrate the increased crack growth rates during stage III that the Forman fit is modeling at room temperature. Due to the linear nature of Paris and Walker model equations, these two cannot predict region III of the FCG experimental data.

Crack Tip Observations

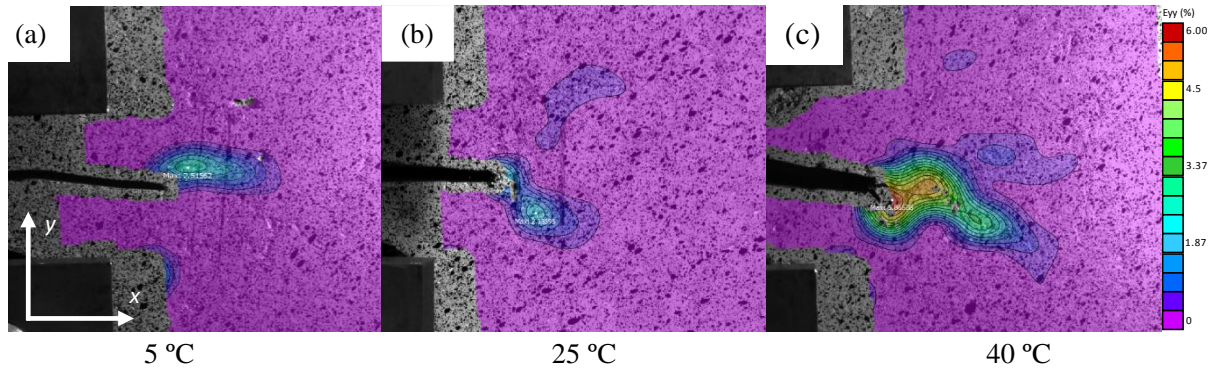


Figure 28 – Vertical strain E_{yy} at crack tip at maximum load during fracture toughness tests at 5, 25, and 40 °C.

Strain fields at the crack tip of each test were obtained using DIC. Vertical strains E_{yy} are obtained during fracture toughness tests at maximum load. Contour profiles are compared for each temperature in percent (%) scale (with each percent equal to 1000 micro strain) as depicted in Figure 28a-c. The average vertical strain, E_{yy} was recorded as 3.00, 2.04, and 4.95% at 5, 25, and 40°C respectively.

It is observed that as the temperature increases, the size of the process zone increases. This is indicated by blunting of the notch tip and increased crack tip opening displacement. In addition, secondary strain concentrations form near the notch tip. Strain concentrations apart from the primary crack at the notch tip are related to the heterogeneity of HMA coupled with mechanical property mismatch [42]. Strain concentrations arise in the matrix where the low modulus of the asphalt allows for more deformation when compared to the aggregate. For temperatures 25 °C and above, as seen in *Yi-qiu* investigation at room temperature, strains away from the crack are related to the distribution of aggregates and asphalt binder. The asphalt binder will create these strain zones due to the lower module compared to the aggregates' while loading [42]. It is found that the distribution of aggregates, air voids near the crack, defects, and micro-cracks will affect the

distribution of strain concentrations. However, for 25 and 40 °C, the maximum points were found at the bridging of the crack and still increasing after the maximum force.

Evolution of Strain Fields

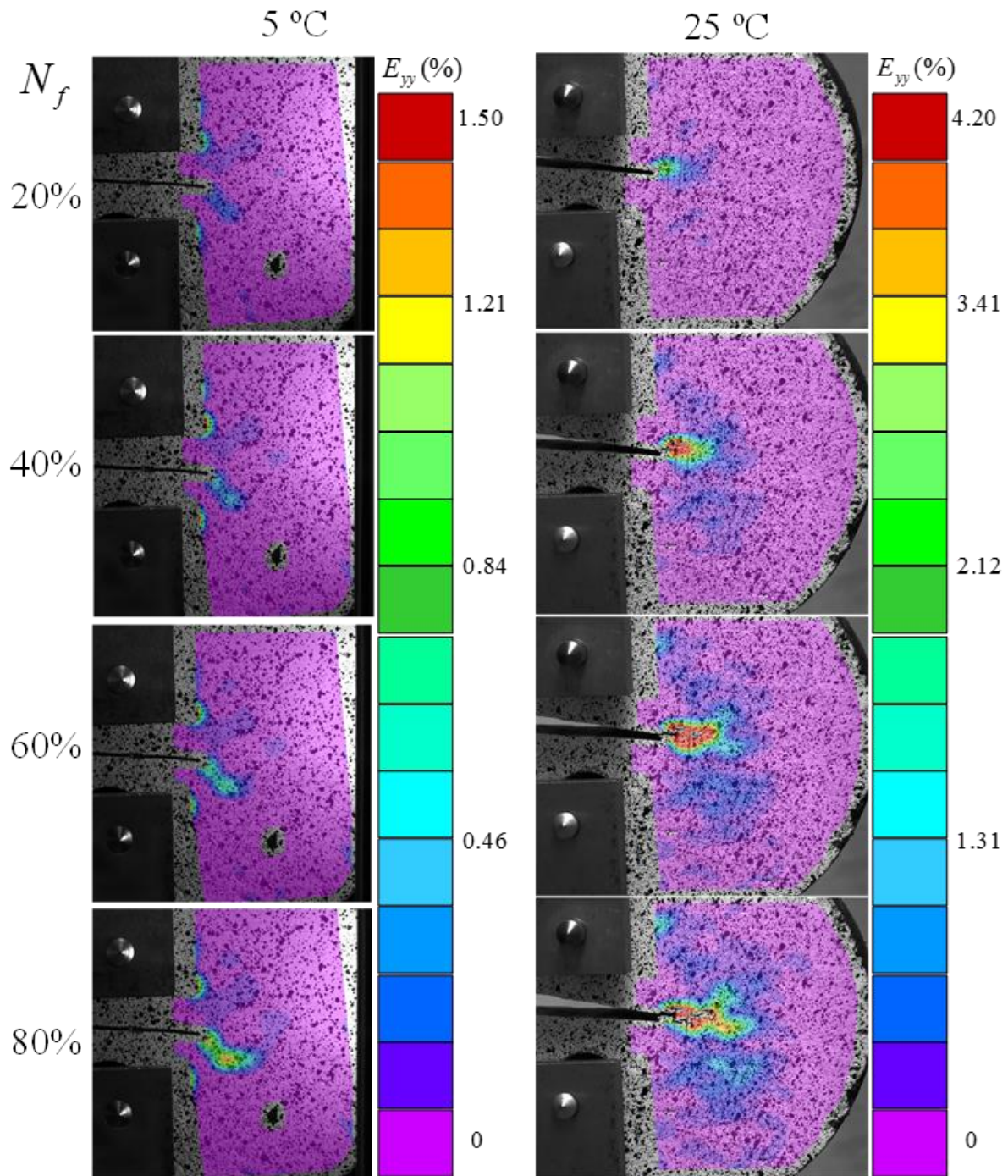


Figure 29 – Vertical strain evolution E_{yy} at different fatigue life percent N_f in specimen at 5 and 25 °C respectively.

Contours of vertical strain, E_{yy} measured during FCG tests are shown in Figure 29. Snapshots are shown at 20, 40, 60, and 80% of the fatigue life. At 5°C the contours range from 0 to 1.5% achieving average K_{ic} at 86.3% fatigue life while at 25°C the contours range from 0 to 4.20% achieving average K_{ic} at 97.32% fatigue life.

For the 5°C FCG test, initial propagation is steady. During the first 60% of fatigue life, no noticeable damage around the crack tip is observed. From 60% to 80%, crack propagation begins at a rapid rate. After 80%, the crack begins to appreciably propagate and shortly after K_{ic} is achieved with fast propagation towards final fracture. Minimum strain concentrations formed around the crack. At this temperature, molecular mobility decreases and thus strain concentrations produced by the stresses occur at the bonding level until breakage where the higher strains and stresses fall onto the neighboring bonds creating the weak zones around the crack [28]. It is difficult to determine the exact point of the crack tip because of the tortuous fracture caused by the aggregate-binder interface in these materials. However, at low temperature more localized strain concentration zones and deformation is observed. No secondary cracks formed during this test and final crack length remained short at 57.88 mm. The maximum vertical strain at fracture is 3.90%. The cracking behavior at 5 °C produces less scattering of data points.

For the FCG 25°C test, most of fatigue life is spent propagating the crack. Stable crack growth started between 0 and 20% of fatigue life. After 40% secondary cracks started to form with torturous growth throughout the fracture area along with ductile fracture. Large damage areas are observed around and away from the crack path. Stresses caused by traffic load produce more plastic deformations due to higher molecular mobility [28]. It is important to note that as cycles increased micro damage and larger strain zones were apparent in the entire specimen. Since this material is a coarse surface mix type it will resist rutting, but these mixes are not meant for fatigue

cracking resistance purposes which is seen in the large process zones [44]. The final crack length was long at 81.18 mm. The maximum vertical strain at fracture is 5.15%.

The DCT configuration favored to determine these results considering the large fracture area and relative low COV during the analysis.

Chapter 6: Summary And Conclusions

For this study, the fracture and fatigue crack growth properties were evaluated for a dense-graded HMA mixture using the DCT configuration. An analysis at different temperatures of fracture and fatigue crack growth parameters and 3D-DIC strain fields during cracking and cycling was performed. The effect of thickness on the fracture resistance of HMA mixtures in the DCT configuration was also evaluated. For dense-grade HMA tested, the following major conclusions were determined:

Regarding fracture

- Checking the requirements of ASTM E399-12 and E1820-16, [Eq. (1)], the specimens are in plane-stress when $B \leq 88$ mm and plane-strain when $B \geq 244$ mm .
- K_c is thickness dependent for specimens with widths of 25 to 75 mm. The COV of K_c is acceptable (at 15% and less) but inconsistent with thickness.
- G_f is independent of thickness for specimens with widths of 25 to 75 mm. The COV of G_f decreases with thickness and is excellent (<5%) at $B \geq 50$ mm. The standard 50 mm thick specimen is adequate when performing G_f test.
- Fracture energy and fracture toughness decrease as temperature increases and there is an increasing trend in COV as temperature increases.
- There is no trend between crack path and thickness. 3D surface scans do not provide enough evidence to determine the plane-stress or plane-strain condition.

Regarding fatigue crack growth

- Following ASTM E399-12 requirements and pre-cracking procedures, results using optical measurements are repeatable with overall reasonable low COVs.

- Fatigue crack growth testing at 40°C was not successful due to the high deformation and large damage zones observed in this material. Fatigue crack length curve exhibit deviations at 25°C and more of a smooth curve at 5 °C Fatigue crack growth rates at 5°C are ten to a thousand times higher than at 25°C.
- Paris and Walker models proved to be optimal falling within the confidence bands of the FCG curve.
- Strain concentrations increase as temperature increases with secondary cracks and damage zones away from the notch tip at 25°C and higher.
- After 60% of fatigue life crack begins to appreciably propagate and rapid rates after 80% at 5 °C. Strain concentrations are focused around the crack tip with minimum damage around it. Most of fatigue life is spent propagating the crack at 25 °C with stable crack growth. Damaged zones are observed around the crack tip as well as secondary cracking after 40% of fatigue life.

Overall, the DCT testing method was proved to be practical and viable method for fracture and fatigue crack growth testing due low variability and repeatability in results. Considering the difficulty to determine the exact point of the crack tip due to the tortuous nature of the fracture, the optical measurement procedure provided repetitive and reliable results. Material variables such as composition, binder, gradation, and asphalt size greatly influence the outcome in results, however the DCT method can contribute in evaluating data for future fatigue crack growth testing. The fracture resistance of each HMA mixture is unique. The functional dependence of factors such as size, thickness, temperature, etc. will change when the composition and gradation are altered.

Future Work

In future work, fracture resistance tests will be performed under service-like conditions including the cracking mode, strain rate, temperature, and layer thickness. Thermo-mechanical fatigue crack growth tests will be designed to simulate (in an accelerated manner) the degradation of HMAs to further understand these complex phenomena in these materials.

References

- 1] Im, S., Ban, H., & Kim, Y. R. (2014). Characterization of mode-I and mode-II fracture properties of fine aggregate matrix using a semicircular specimen geometry. *Construction and Building Materials*, 52, 413-421.
- 2] Tschegg, E. K., Jamek, M., & Lugmayr, R. (2011). Fatigue crack growth in asphalt and asphalt-interfaces. *Engineering Fracture Mechanics*, 78(6), 1044-1054.
- 3] Lytton, R. L., Zhang, Y., Luo, X., & Luo, R. (2015). The fatigue cracking of asphalt mixtures in tension and compression.
- 4] Nejad, F. M., Aflaki, E., & Mohammadi, M. A. (2010). Fatigue behavior of SMA and HMA mixtures. *Construction and Building Materials*, 24(7), 1158-1165.
- 5] Saha, G., & Biligiri, K. P. (2016). Homothetic behaviour investigation on fracture toughness of asphalt mixtures using semicircular bending test. *Construction and Building Materials*, 114, 423-433.
- 6] Saha, G., & Biligiri, K. P. (2016). Fracture properties of asphalt mixtures using semi-circular bending test: a state-of-the-art review and future research. *Construction and Building Materials*, 105, 103-112.
- 7] Alataş, T., Yılmaz, M., Kök, B. V., & fatih Koral, A. (2011). Comparison of permanent deformation and fatigue resistance of hot mix asphalts prepared with the same performance grade binders. *Construction and Building Materials*, 30, 66-72.
- 8] Krishnan, J. M., and Rajagopal, K. R., 2005, "On the Mechanical Behavior of Asphalt," *Mechanics of Materials*, 37(11), pp. 1085-1100.
- 9] Wagoner, M., Buttlar, W., Paulino, G., & Blankenship, P. (2005). Investigation of the fracture resistance of hot-mix asphalt concrete using a disk-shaped compact tension test. *Transportation Research Record: Journal of the Transportation Research Board*, (1929), 183-192.
- 10] Aliha, M. R. M., Bahmani, A., & Akhondi, S. (2016). A novel test specimen for investigating the mixed mode I+ III fracture toughness of hot mix asphalt composites—Experimental and theoretical study. *International Journal of Solids and Structures*, 90, 167-177.
- 11] Stewart, C. M., Reyes, J. G., & Garcia, V. M. (2017). Comparison of fracture test standards for a super pave dense-graded hot mix asphalt. *Engineering Fracture Mechanics*, 169, 262-275.
- 12] Kim, H., Wagoner, M. P., & Buttlar, W. G. (2009). Numerical fracture analysis on the specimen size dependency of asphalt concrete using a cohesive softening model. *Construction and Building Materials*, 23(5), 2112-2120.

- 13] Aliha, M. M., Behbahani, H., Fazaeli, H., & Rezaifar, M. H. (2014). Study of characteristic specification on mixed mode fracture toughness of asphalt mixtures. *Construction and Building Materials*, 54, 623-635.
- 14] Li, X., & Marasteanu, M. (2010). The fracture process zone in asphalt mixture at low temperature. *Engineering Fracture Mechanics*, 77(7), 1175-1190.
- 15] Behbahani, H., Aliha, M., Reza, M., Fazaeli, H., & Aghajani, S. (2013). Experimental fracture toughness study for some modified asphalt mixtures. In *Advanced Materials Research* (Vol. 723, pp. 337-344). Trans Tech Publications.
- 16] Braham, A., Buttlar, W., & Marasteanu, M. (2007). Effect of binder type, aggregate, and mixture composition on fracture energy of hot-mix asphalt in cold climates. *Transportation Research Record: Journal of the Transportation Research Board*, (2001), 102-109.
- 17] Braham, A., and Underwood, B. S., 2016, *State of the Art and Practice in Fatigue Cracking Evaluation of Asphalt Concrete Pavements*.
- 18] Kim, K. W., & El Hussein, M. (1997). Variation of fracture toughness of asphalt concrete under low temperatures. *Construction and building Materials*, 11(7-8), 403-411.
- 19] Zegeye, E., Le, J. L., Turos, M., & Marasteanu, M. (2012). Investigation of size effect in asphalt mixture fracture testing at low temperature. *Road Materials and Pavement Design*, 13(sup1), 88-101.
- 20] Li, X., & Marasteanu, M. (2010). The fracture process zone in asphalt mixture at low temperature. *Engineering Fracture Mechanics*, 77(7), 1175-1190.
- 21] Molenaar, A. A. A., Scarpas, A., Liu, X., & Erkens, S. M. J. G. (2002). Semi-circular bending test; simple but useful?. *Journal of the Association of Asphalt Paving Technologists*, 71.
- 22] Sanford, R.J. *Principles of Fracture Mechanics*, first ed., Upper Saddle River, New Jersey, 2003.
- 23] AASHTO. TP105-13 Standard method of test for determining the fracture energy of asphalt mixtures using the semi circular bend geometry (SCB) 2013:1-14.
- 24] ASTM Standard D7313, 2007 (2013), " Standard Test Method for Determining Fracture Energy of Asphalt-Aggregate Mixtures Using the Disk-Shaped Compact Tension Geometry," ASTM International, West Conshohocken, PA, 2013, DOI: 10.1520/D7313-13.
- 25] Arabani, M., & Ferdowsi, B. (2009). Evaluating the semi-circular bending test for HMA mixtures. *International Journal of Engineering A: Basics*, 22(1), 47-58.
- 26] ASTM Standard E399, 1970 (2012), " Standard Test Method for Linear-Elastic Plane-Strain Fracture Toughness K_{Ic} of Metallic Materials," ASTM International, West Conshohocken, PA, 2013, DOI: 10.1520/E399-12E03.

- 27] ASTM E1820-16, Standard test method for measurement of fracture toughness, ASTM International, West Conshohocken, PA, 2016, www.astm.org, doi:10.1520/E1820-16.
- 28] Moreno-Navarro, F., & Rubio-Gámez, M. C. (2016). A review of fatigue damage in bituminous mixtures: Understanding the phenomenon from a new perspective. *Construction and Building Materials*, 113, 927-938.
- 29] Behnia, B., Dave, E., Ahmed, S., Buttlar, W., & Reis, H. (2011). Effects of recycled asphalt pavement amounts on low-temperature cracking performance of asphalt mixtures using acoustic emissions. *Transportation Research Record: Journal of the Transportation Research Board*, (2208), 64-71.
- 30] Aliha, M. R. M., Bahmani, A., & Akhondi, S. (2015). Determination of mode III fracture toughness for different materials using a new designed test configuration. *Materials & Design*, 86, 863-871.
- 31] Zhou, F., Hu, S., and Scullion, T. (2007). "Development and verification of the overlay tester based fatigue cracking prediction approach." FHWA/ TX-07/9-1502-01-8, Texas Transportation Institute, College Station, Texas.
- 32] Zhou, F., and Scullion, T. (2003). "Upgraded overlay tester and its application to characterize reflection cracking resistance of asphalt mixtures" FHWA/ TX-04/0-4467-1, Texas Transportation Institute, College Station, Texas
- 33] Khiavi, A. K., & Ameri, M. (2014). Investigating the fatigue endurance limit of HMA mixture using RDEC approach. *Construction and Building Materials*, 55, 97-102.
- 34] Fakhri, M., Ghanizadeh, A. R., & Omrani, H. (2013). Comparison of fatigue resistance of HMA and WMA mixtures modified by SBS. *Procedia-Social and Behavioral Sciences*, 104, 168-177.
- 35] AASHTO. T312-15 Preparing and Determining Density of Hot Mix asphalt (HMA) Specimens by Means of the Superpave Gyratory Compactor 2015:1–6.
- 36] ASTM Standard D6928, 2003 (2015), "Standard Test Method for Preparation and Determination of the Relative Density of Asphalt Mix Specimens by Means of the Superpave Gyratory Compactor," ASTM International, West Conshohocken, PA, 2013, DOI: 10.1520/D6925-15.
- 37] Rasband, W.S., 1997-2016, ImageJ, U. S. National Institutes of Health, Bethesda, Maryland, USA, <http://imagej.nih.gov/ij/>.
- 38] ASTM Standard E647, 1978 (2015), " Standard Test Method for Measurement of Fatigue Crack Growth Rates," ASTM International, West Conshohocken, PA, 2013, DOI: 10.1520/E0647-15E01.
- 39] Zofka, A., & Marasteanu, M. (2006). Development of double edge notched tension (DENT) test for asphalt binders. *Journal of Testing and Evaluation*, 35(3), 1-7.

- 40] Edwards, M., & Hesp, S. (2006). Compact tension testing of asphalt binders at low temperatures. *Transportation Research Record: Journal of the Transportation Research Board*, (1962), 36-43.
- 41] Aliha, M. R. M., Fazaeli, H., Aghajani, S., & Nejad, F. M. (2015). Effect of temperature and air void on mixed mode fracture toughness of modified asphalt mixtures. *Construction and Building Materials*, 95, 545-555.
- 42] Yi-qiu, T., Lei, Z., Meng, G., & Li-yan, S. (2012). Investigation of the deformation properties of asphalt mixtures with DIC technique. *Construction and Building Materials*, 37, 581-590.
- 43] ASTM Standard D6931, 2007 (2012), " Standard Test Method for Indirect Tensile (IDT) Strength of Bituminous Mixtures," ASTM International, West Conshohocken, PA, 2013, DOI: 10.1520/D6931-12.
- 44] Zhang, J., Simate, G. S., Lee, S. I., Hu, S., & Walubita, L. F. (2016). Relating asphalt binder elastic recovery properties to HMA crack modeling and fatigue life prediction. *Construction and Building Materials*, 111, 644-651.

Vita

Eduardo Garcia was born on November 14th, 1991 in Torreon, Coahuila, Mexico. He moved to Ciudad Juarez, Chihuahua at age seven. He began his college studies in El Paso, Texas at El Paso Community College and then enrolled in The University of Texas at El Paso, where he completed his Bachelor of Science in Mechanical Engineering in May 2015 and graduated with a Cum Laude honors recognition. He received an invitation from the Mechanical Engineering Department to pursue graduate college, he began in August 2015 under the supervision of Dr. Calvin Stewart. During his graduate studies, he was a teacher assistant and graduate research assistant. He contributed in different projects such as the development of multi-walled carbon-nanotube- based alginate hydrogels where he is a published author. He also investigated the stress corrosion cracking of aluminum foils. He is a member of The American Society of Mechanical Engineers (ASME). During his master's degree, he was part of a project funded by The Southern Plains Transportation Center where he devoted his research work in the fracture and fatigue crack growth rate of hot mix asphalts. After graduation, Eduardo will seek and pursue a career in Mechanical Engineering in the industry.

Permanent address: Montebello 2445, Fracc. Los Manantiales 16-C,
Ciudad Juarez, Chihuahua, Mexico, 32538.

This thesis was typed by Eduardo Garcia.